Biochimica et Biophysica Acta 1794 (2009) 634–641

Contents lists available at ScienceDirect

Biochimica et Biophysica Acta

journal homepage: www.elsevier.com/locate/bbapap

Altered chain-length and glycosylation modify the pharmacokinetics of human serum albumin

Yasunori Iwao [a], Mikako Hiraike [a], Ulrich Kragh-Hansen [b], Keiichi Kawai [c], Ayaka Suenaga [a], Toru Maruyama [a], Masaki Otagiri [a,*]

[a] Department of Biopharmaceutics, Graduate School of Pharmaceutical Sciences, Kumamoto University, 5-1 Oe-honmachi, Kumamoto 862-0973, Japan
[b] Department of Medical Biochemistry, University of Aarhus, DK-8000 Aarhus C, Denmark
[c] School of Health Sciences, Faculty of Medicine, Kanazawa University, Ishikawa 920-0942, Japan

ARTICLE INFO

Article history:
Received 19 September 2008
Accepted 3 November 2008
Available online 8 December 2008

Keywords:
Human serum albumin
Genetic variant
Pharmacokinetics
Half-life
Hepatic uptake
Renal disposition
Spleen uptake

ABSTRACT

Human serum albumin with modified plasma half-life will be useful for clinical purposes. Therefore, the pharmacokinetics of three of each of the following types of genetic variants, and of their corresponding normal albumin, were examined in mice: N-terminally elongated, C-terminally truncated and glycosylated albumins. Isoforms differing from the normal protein by three or more amino acids, especially two of the truncated forms, had shorter half-lives. The effect of glycosylation depended on the position of attachment: in domain II it increased half-life, whereas in domain I and III it had no significant effect. Liver, kidney and spleen uptake clearances were also modified. The pronounced changes in half-life of the two truncated variants and the glycosylated isoform could be explained, at least partly, by large changes in organ uptakes; in the remaining six cases, different effects were registered. Such information should be useful when designing therapeutical albumin products for, e.g., drug delivery systems. In addition to various types of cell endocytosis, leading to intracellular destruction or recycling of the proteins, the metabolism of the alloalbumins could be affected by plasma enzymes. No correlation was found between mutation-induced changes in the pharmacokinetic parameters and changes in α-helical content or changes in heat stability as represented by ΔH_v.

1. Introduction

Human serum albumin (HSA) is produced in the parenchymal cells of the liver, and it is the most abundant plasma protein. It is an important circulating depot protein and transport protein for endogenous and exogenous ligands in the blood, and contributes to the maintenance of osmotic pressure, plasma pH and to the Donnan-effect in the capillaries [1,2]. The protein is formed by a single polypeptide chain of 585 amino acids, and it has a molecular mass of approximately 66.5 kDa [2]. According to X-ray crystallographic analyses of HSA and of its recombinant version (rHSA), albumin has about 67% α-helix but no β-sheet. The analyses also showed that the polypeptide chain forms a heart-shaped protein with three homologous domains (I–III), each comprised of two subdomains (A and B) with distinct helical folding patterns that are connected by flexible loops [3,4]. A combined phosphorescence depolarization-hydrodynamic modeling study has proposed that the overall conformation of HSA in neutral solution is very similar to that observed in the crystal form [5].

Clinically, HSA is used for urgent restoration of blood volume, emergency treatment of chock, acute management of burns and other situations associated with hypoproteinemia [2]. To date, albumin has been produced by fractionation of whole blood. However, there is the potential risk of HSA contamination with blood-derived pathogens. In addition, human plasma can be in limited supply. Because of these problems, rHSA, which is highly expressed by *Pichia pastoris*, most probably will be commercially available in the near future [6]. Another benefit of this approach is that protein engineering will enable the creation of rHSAs with modified properties such as extended half-life in the circulation. In this connection HSA dimers seem to be useful candidates. Matsushita et al. [7] found that rHSA dimers had a high retention rate in the circulatory blood and a lower vascular permeability than native rHSA in normal rats and in mice with paw edema. Similar observations have been made by Komatsu et al. [8], who examined the pharmacokinetics of chemically crosslinked rHSA dimers in the rat. On the other hand, recombinant albumin domain(s) are cleared very fast. Sheffield et al. [9] found that recombinant domain I, I+II and III of rabbit serum albumin all had very short mean terminal catabolic half-lives in rabbits due to a fast elimination in the urine.

Abbreviations: HSA, human serum albumin; rHSA, recombinant HSA; Alb, albumin; Alb A, normal (wild-type) albumin; CD, circular dichroism; ΔH_v, van't Hoff enthalpy; RAGE, receptor for advanced glycation end products

* Corresponding author. Tel.: +81 96 371 4150; fax: +81 96 362 7690.
E-mail address: otagirim@gpo.kumamoto-u.ac.jp (M. Otagiri).

1570-9639/$ – see front matter © 2008 Elsevier B.V. All rights reserved.
doi:10.1016/j.bbapap.2008.11.022

Because of a relatively high in vivo half-life of ca. 19 days [2], HSA is an attractive fusion partner to extend the half-life, and potentially the therapeutic utility, of recombinant peptides and proteins. Among recent examples are rHSA genetically fused to type 1 interferons [10], glucagon-like peptide-1 [11] and interleukin-2 [12]. However, although an extension of the half-life of therapeutic peptides and proteins often is desirable, an extension to that of albumin could be excessive.

Although HSA-preparations with a modified half-life thus could be very useful, not much has been done to design or find such preparations. In our search for useful candidates, we have paid our attention to HSA genetic variants. Until now, 65 inherited variants of HSA, including proalbumin variants, have been identified and structurally characterized [13]. Usually, these genetic variants are expressed in heterozygous form and without any known association to disease [13]. Therefore, unlike lethal mutations, such may occur for hemoglobin and coagulation factors, studying the pharmacokinetic properties of HSA variants is a good way of gaining information which can be used when designing recombinant HSAs, because we can consider the effects of molecular variation without worrying about complications such as antigenic effects.

Recently, we have studied the pharmacokinetic properties in mice of 17 alloalbumins with single-residue mutations [14]. The study showed that, for example, only a few of the variants had a significantly modified half-life in the blood. In an attempt to find genetic variants with a more pronounced impact on pharmacokinetics, we now have expanded that study by determining the plasma half-lives and organ uptakes of three HSAs with a slightly longer chain-length (proalbumin variants), three with a slightly shorter chain-length (C-terminal variants) and three alloalbumins *N*-glycosylated in domain I, II and III, respectively. For being able to make a more detailed comparison between molecular characteristics and pharmacokinetic properties, we have estimated the effect of the molecular modifications on the α-helical content of the alloalbumins by using circular dichroism (CD). Previously, the effect of genetic variation on the thermal stability of HSA has been quantified in terms of, for example, changes in the van't Hoff enthalpy (ΔH_v) [15]. In the present work, the pharmacokinetic results have also been related to changes in ΔH_v.

2. Materials and methods

2.1. Protein samples

The genetic variants of HSA and their normal (wild-type) counterpart (endogenous Alb A) were isolated from serum from heterozygous carriers by ion-exchange chromatography. The locations of the structural changes of the nine variants are indicated in Fig. 1. After isolation, the albumins were checked for homogeneity by native electrophoresis, and no denaturation or significant (no more than 5%) cross-contamination between variant and Alb A was detected. The proteins were donated to us by Drs. M. Galliano and L. Minchiotti, University of Pavia, Pavia, Italy; Dr. S.O. Brennan, Canterbury Health Laboratories, Christchurch, New Zealand; and Dr. D. Donaldson, East Surrey Hospital, Redhill, UK. Before use, the albumins were delipidated by treatment with hydroxyalkoxypropyldextran at pH 3.0, as described in a previous paper [16]. After defatting, the albumins were dialysed extensively against deionized water, lyophilized and stored at −20 °C until used. Thus, the albumins from a donor have been exposed to exactly the same conditions from the time the blood samples were taken until the present experiments were performed.

Fraction V HSA (96% pure), assumed to be Alb A, was donated by the Chemo-Sera-Therapeutic Research Institute (Kumamoto, Japan) and defatted using the charcoal procedure described by Chen [17], deionized, freeze-dried and then stored at −20 °C until used.

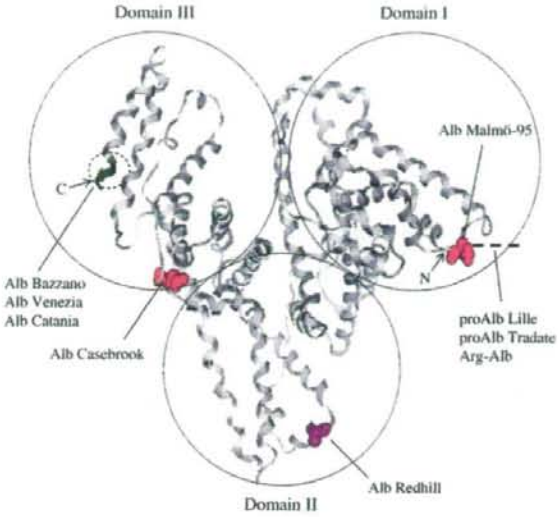

Fig. 1. The crystal structure of HSA indicating the locations of the mutations of the three C-terminal variants and the three proAlb variants used in this study. The locations of the glycosylated 63 Asn (Alb Malmö-95), 318 Asn (Alb Redhill) and 494 Asn (Alb Casebrook) are also shown. The subdivision of HSA into domains is marked; N and C stand for the N-terminal and the C-terminal ends, respectively. The broken, black line added to the N-terminal end indicates the prosegment of HSA.

2.2. Chemicals and animals

$^{111}InCl_3$ (74 Mbq/mL in 0.02 N HCl) was donated by Nihon Medi-Physics (Takarazuka, Japan). All chemicals were of the highest grade commercially available, and all solutions were prepared using deionized, distilled water.

Male ddY mice (26–32 g) were purchased from the Shizuoka Agricultural Cooperative Association for Laboratory Animals (Shizuoka, Japan), and were maintained under conventional housing conditions. All animal experiments were conducted in accordance with the principles and procedures outlined in the National Institute of Health Guide for the Care and Use of Laboratory Animals.

2.3. In vivo experiments

All proteins were radiolabeled with ^{111}In using the bifunctional chelating reagent DTPA anhydride according to the method of Hnatowich et al. [18], as described elsewhere [19]. In previous works, we found no significant differences in pharmacokinetic properties among these albumins, when ^{111}In-labeled mouse, rat, bovine or human serum albumin was administered to mice (unpublished), suggesting that immunogenic behavior does not occur in mice. Therefore, we chose the mouse as a reasonable model for the study of the pharmacokinetics of the HSAs. Mice received tail vein injections of ^{111}In-labeled proteins in saline, at a dose of 0.1 mg/kg and were housed in metabolic cages to allow the collection of urine samples. Urine samples were collected throughout the 120 min of the experimental period. In the early period after injection, the efflux of ^{111}In radioactivity from organs is assumed to be negligible, because the degradation products of ^{111}In-labeled proteins using DTPA anhydride cannot easily pass through biological membranes [20]. This assumption was supported by the fact that no ^{111}In was detectable in the urine after 120 min. At 1, 3, 5, 10, 30, 60, 90 or 120 min after injection, blood was collected from the vena cava under ether anesthesia and plasma was obtained by centrifugation. After blood collection, the animals were sacrificed, organs were excised, rinsed with saline and weighed.

The radioactivity of each blood and tissue sample was measured in a well-type NaI scintillation counter (ARC-500, Aloka, Tokyo).

Pharmacokinetic analyses were performed as follows. The plasma ^{111}In radioactivity concentrations (C_p) were normalized with respect to the percentage of injected dose and analyzed using the nonlinear least-square program MULTI [21]. The two-compartment model was fitted according to the Akaike information criterion by Eq. (1).

$$C_p = Ae^{-\alpha t} + Be^{-\beta t} \quad (1)$$

The half-lives of the HSAs were determined as β-phase elimination within a 120-min period. The tissue distribution patterns were evaluated using tissue uptake clearances (CL_{uptake}) according to the integration plot analysis. CL_{uptake} was calculated using Eq. (2).

$$CL_{uptake} = \frac{X_t/C_t}{AUC_{0-t}/C_t} \quad (2)$$

where X_t is the tissue accumulation at time t, AUC_{0-t} is the area under the plasma concentration time-curve from time 0 to t, and C_t is the plasma concentration at time t. CL_{uptake} was obtained from the slope of the plot of X_t/C_t versus AUC_{0-t}/C_t. We estimated the organ uptake clearances within a 30 min period.

2.4. Far-UV CD spectra

The protein concentration was 1.5 μM, as determined by the method of Bradford [22], and the buffer was 67 mM sodium phosphate, pH 7.4, 25 °C. Far-UV intrinsic spectra were recorded from 200 to 250 nm using a Jasco J-720 spectropolarimeter (Tokyo, Japan). For calculation of the mean residue ellipticity, [θ], the molecular masses were assumed to be 65.8 kDa for Alb Venezia, 67.1 kDa for proAlb Lille and Tradate and 66.5 kDa for the remaining variants and Alb A. The α-helical content of the proteins was estimated from the ellipticity values at 222 nm as described by Chen et al. [23].

2.5. Analysis of experimental data

The effects of the molecular changes were evaluated by using the following relationship:

$$\text{Percent change} = \frac{(\text{Result for variant}) - (\text{Result for Alb A})}{(\text{Result for Alb A})} \times 100\% \quad (3)$$

In Eq. (3), the result can be a value determined for plasma half-life, organ uptake clearance, α-helical content or for ΔH_u.

2.6. Statistical analysis

Statistical analyses were performed by using the Student t-test. A probability value of $P<0.05$ was considered to indicate statistical significance.

3. Results

3.1. The genetic variants

The alloalbumins used in this study have been named after the place from where the first detected carrier originates, and their molecular changes are summarized in Table 1.

Proalbumin (proAlb) is an albumin molecule to which the propeptide, Arg-Gly-Val-Phe-Arg-Arg-, is still bound at the N-terminus (Fig. 1). The positions of the propeptide are numbered from −6 to −1 (the juxtaposition to albumin). Normally, proAlb does not occur in detectable amounts in the circulation, because the propeptide is cleaved off by propeptidase within the liver cells. However, substitution of −1 Arg or −2 Arg (as in proAlb Lille [24] and proAlb Tradate [25]) inhibits the proteolytic cleavage of the propeptide but not the secretion of the protein, and such proalbumin variants, in contrast to wild-type proalbumin, can be isolated from the serum. In vivo, the prepro-form of proAlb Tradate (−2 Arg→Cys) is often cleaved after the mutated residue giving rise to HSA retaining −1 Arg (Arg-Alb) [25].

Among the C-terminal variants most are truncated albumins (Table 1). Thus, Alb Catania is three amino acids shorter than Alb A, and the three last residues in the new C-terminal end are changed from Gln-Ala-Ala to Lys-Leu-Pro [26]. Alb Venezia has been shortened by seven amino acids, and the new C-terminal end is changed from Gly-Lys-Lys-Leu-Val-Ala-Ala to Pro-Thr-Met-Arg-Ile-Arg-Glu [26]. Alb Bazzano has been shortened by three amino acids, and 14 of the last 16 amino acids in the new C-terminal end have been substituted: from Cys-Phe-Ala-Glu-Glu-Gly-Lys-Lys-Leu-Val-Ala-Ala-Ser-Gln-Ala-Ala to Ala-Leu-Pro-Arg-Arg-Val-Lys-Asn-Leu-Leu-Leu-Gln-Val-Lys-Leu-Pro [27]. Here the 567 Cys→Ala substitution has caused the loss of the C-terminal disulfide bridge.

It is uncommon for an amino acid substitution to result in the formation of an oligosaccharide attachment sequence. However, that has happened to Alb Malmö-95 [28], Alb Redhill [29,30] and Alb Casebrook [31,32], which are glycosylated in domain I, II and III, respectively (Fig. 1). In all three cases, the glycan is a disialylated (mainly or totally) biantennary complex type oligosaccharide N-linked to an asparagine residue [30]. Alb Redhill is unique, because it is

Table 1
Half-lives and organ uptake clearances of ^{111}In-labeled HSA variants and corresponding Alb A in mice

Variant name (mutation)	Domain		Half-life[a] (min)	Clearance (μL/hr)[a]		
				Liver	Kidney	Spleen
proAlb Lille (−2Arg->His)	I	Variant	251.1±4.31*	56.13±8.07	60.06±6.76	82.47±15.96
		Alb A	264.3±4.58	42.66±7.52	79.69±8.04	90.11±7.97
proAlb Tradate (−2Arg->Cys)	I	Variant	249.4±5.89	111.99±14.99	89.14±11.11**	74.83±13.57
		Alb A	252.4±7.62	109.99± 14.01	46.01±6.89	87.86±6.36
Arg-Alb (Alb A having −1 Arg)	I	Variant	262.1±6.53	21.16±3.72**	99.98±23.18	105.77±14.52
		Alb A	253.5±4.98	94.38±5.17	119.38±10.29	91.38±6.51
Alb Bazzano (567–582 substituted, 583–585 deleted)	III	Variant	231.1±5.31*	189.77±26.11**	253.69±36.22**	84.66±7.00**
		Alb A	245.2±6.93	41.35±4.68	119.95±20.05	57.94±5.11
Alb Venezia (572–578 substituted, 579–585 deleted)	III	Variant	225.1±5.49**	134.32±11.41**	136.11±13.55**	88.48±10.15
		Alb A	247.2±6.83	41.24±4.81	62.87±3.28	67.89±15.03
Alb Catania (580–582 substituted, 583–585 deleted)	III	Variant	248.6±5.46	12.29±1.18*	140.09±15.01**	45.97±5.15
		Alb A	251.3±3.99	48.99±18.18	81.53±12.02	52.69±7.64
Alb Malmö-95 (63 Asp->Asn, glycosylated at 63 Asn)	I	Variant	261.3±7.62	145.82±13.84**	113.96±15.72	53.21±4.21**
		Alb A	264.2±6.14	79.72±11.74	111.64±18.18	82.68±4.09
Alb Redhill (−1 Arg retained, 320 Ala->Thr, glycosylated at 318 Asn)	II	Variant	260.3±7.43*	25.69±3.51**	62.62±7.05**	45.68±6.91**
		Alb A	245.2±6.34	93.49±8.95	125.84±15.21	84.39±7.26
Alb Casebrook (494 Asp->Asn, glycosylated at 494 Asn)	III	Variant	251.2±4.88	134.79±13.97**	141.01±8.14	56.94±6.10
		Alb A	249.1±4.54	81.45±9.19	148.71±21.18	57.73±4.25

[a] The data are average values of 3–6 experiments (±SD). *$P<0.05$, **$P<0.01$ as compared with endogenous Alb A.

the only example so far of an albumin with two mutations. One is the 320 Ala→Thr, which leads to glycosylation of 318 Asn; the other is −2 Arg→Cys, which results in abnormal hydrolysis of the prepro-form within the liver cells and to the formation of albumin still possessing −1 Arg [29].

According to the literature cited [24–32], none of the mutations seem to affect the oligomeric state of albumin.

3.2. Pharmacokinetic properties of HSA variants

Fig. 2 shows the time courses for radioactivity in mouse plasma after intravenous administration of ^{111}In-labeled preparations of the variants and their corresponding Alb A. As seen, in all 9 cases the mutation affected, to different degrees, the elimination of HSA. Table 1 gives the plasma half-lives, calculated by β-phase using the nonlinear least-square program MULTI and Eq.(1), and liver, kidney and spleen uptake clearances, determined by an integration plot analysis (Eq.(2)). As a control we have compared the pharmacokinetic results obtained for endogenous Alb A (Table 1) with those obtained with commercial HSA (not illustrated), because both types of preparations are assumed to represent the normal protein. The average half-lives for Alb A and commercial HSA are 252.5 min and 268.2±7.2 min (n=6), respectively. The liver, kidney and spleen uptake clearances for Alb A are on an average 70.36 μL/h, 99.51 μL/h and 74.74 μL/h, respectively, whereas

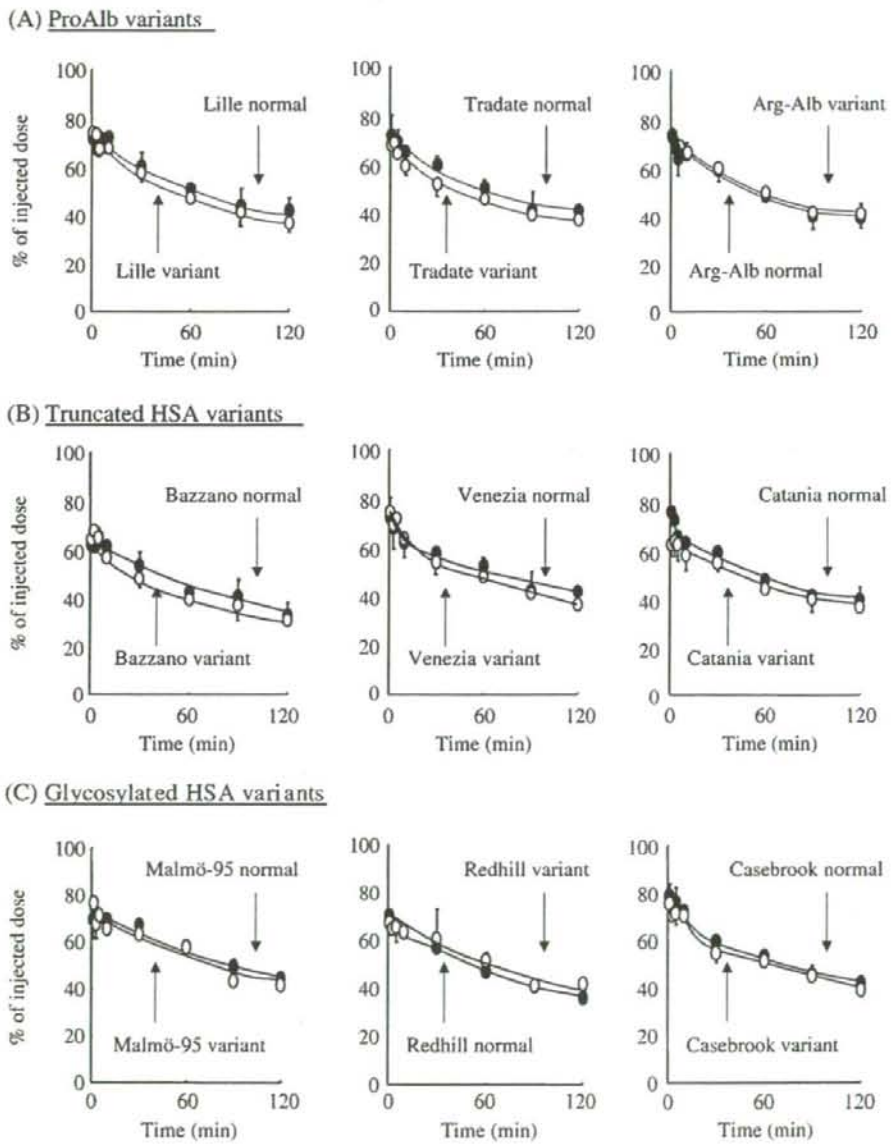

Fig. 2. Relative plasma amounts of ^{111}In-labeled proAlb variants (A), truncated HSA variants (B) and glycosylated HSA variants (C) and their corresponding Alb A after intravenous administration in mice. ^{111}In-albumin was injected as a bolus dose into the tail vein. Relative amounts are plotted against time after injection. The open and closed circles represent variant and normal albumin, respectively. Each point represents an average value obtained for 3–6 mice (±SD).

those for commercial HSA are 54.31±8.23 μL/h, 83.12±5.43 μL/h and 63.65±3.56 μL/h, respectively. The slightly lower half-life and the slightly higher organ uptake clearances found for Alb A are most probably due to differences in isolation and/or defatting procedures.

The effects of the mutations on plasma half-lives and organ uptake clearances, calculated according to Eq.(3), are given in Table 2. As seen, all the proAlb variants and the truncated variants have diminished plasma half-lives, i.e., negative percent changes; this is most evident for Alb Venezia. By contrast, the effect of glycosylation varied: Almost no effect in the case of Alb Malmö-95 and Casebrook but a significant prolongation of the half-life for Alb Redhill. The increase of the half-life for Alb Redhill can partly be explained by the presence of −1 Arg (Table 2). In all 9 cases, the molecular changes resulted in a modified liver, kidney and spleen uptake clearance (Table 2). The most pronounced effects were found for the truncated variants Alb Bazzano and Venezia; the uptakes by the three organs were increased very much. At the other extreme, the uptakes of Alb Redhill were in all cases significantly decreased. For all three variants, the changes in organ uptakes can explain, at least partly, the changes in plasma half-lives. For the remaining six alloalbumins, the effects on organ uptakes are more complex, i.e., both increases and decreases in uptake were found for the same variant. The most pronounced changes, i.e., more than 100%, were observed for liver and kidney uptakes of Alb Bazzano and Venezia.

3.3. Relationships between structure, stability and pharmacokinetic properties of HSA variants

The effects of genetic variation on the albumin structure were studied by far-UV intrinsic CD. From Fig. 3 it is apparent that the variants have spectra which differ to varying extents from that of their corresponding Alb A. In most cases, the structural modification results in a less negative spectrum. However, in two cases (Arg-Alb and Alb Venezia) the variant has a more negative spectrum. The most pronounced spectral changes were found for two variants having a modified chain length (proAlb Tradate and Alb Bazzano). We used the ellipticities at 222 nm to calculate the α-helical content of all the albumins. The impact of genetic variation on that parameter is given in a quantitative way in Table 2. Because the alloalbumins had both modified pharmacokinetic properties (section 3.2.) and modified α-helical contents we investigated, whether there is a direct correlation between these parameters. That was found not to be the case. When plotting the changes in half-lives as a function of changes in α-helical content a poor correlation was found; a straight line had a P-value of 0.48 (not shown). Likewise, no correlations were found between the changes in organ uptake clearances and changes in α-helical content; the P-values were in the range 0.16–0.52 (not shown).

Previously, we have studied the effects of genetic variation on the thermal stability of HSA [15]. The stability was quantified by determining van't Hoff enthalpies (ΔH_v-values), and the results of that study are included in Table 2. We also examined whether a correlation exists between changes in the ΔH_v-values and the changes in pharmacokinetic properties. However, no such correlation was found. When plotting the changes in half-lives versus the changes in ΔH_v-values, the P-value was only 0.68 (not shown). In addition, no correlations were found between the changes in organ uptakes and changes in ΔH_v-values; the P-values were in the range 0.38–0.83 (not shown).

4. Discussion

Clinically, it would be useful, if protein engineering could result in the production of rHSA preparations with a prolonged half-life in the circulation. In addition, because of its half-life of 19 days in humans, its ease of synthesis and its known structure albumin is an attractive candidate for use in recombinant fusion proteins and as a carrier in drug delivery systems. However, also in the two latter types of examples it would be advantageous to be able to modify the plasma half-life of the protein product. For finding such isoforms, in the present study, we investigated the half-life and organ uptakes of a series of genetic HSA variants with relatively large molecular changes, i.e., modified chain-length or glycosylated. The most clear results were obtained for two truncated alloalbumins (Alb Venezia and Bazzano) and a glycosylated variant (Alb Redhill). For the other six variants less clear and individual results were obtained.

All the alloalbumins with chain-lengths deviating by three or more residues from Alb A have diminished half-lives in the circulation (Table 2). This is most evident for Alb Bazzano and Venezia the half-lives of which were reduced by 6–9%. These results must be due to mutation induced changes in protein charge and/or conformation. In this connection it is relevant to note that Alb Bazzano has lost its C-terminal disulfide bridge because of the 567 Cys→Ala substitution (see Section 3.1.). Our previous study [14], making use of single-residue mutations, revealed that the half-life of Alb Hawkes Bay is shortened by ca. 30%. This finding is due to the mutation 177 Cys→Phe [33], which results in the loss of the disulfide bond between 168 Cys and 177 Cys. Thus, the lifespan of HSA is dependent on the existence of its 17 stabilizing disulfide bridges [1–4].

The effect of glycosylation depends on the position of attachment. Glycosylation of 63 Asn in domain I (Alb Malmö-95) or 494 Asn in domain III (Alb Casebrook) has no significant effect on variant half-life. By contrast, glycosylation of 318 Asn in domain II (Alb Redhill) results in a significant increase in half-life; however, part of the increment is caused by the presence of −1 Arg. Sheffield et al. [9] also observed position-dependent effects of N-glycosylation when studying the half-life of mutated rabbit serum albumin in rabbits. These authors reported no effect of glycosylation of 12 Asn in the 14 Val→Thr variant. By contrast, a similar modification of 494 Asn in the 494 Asp→Asn isoform resulted in a reduction of the mean terminal catabolic half-life from 4.32 days to 2.87 days. The different results obtained in our and their study for the latter variant is probably due to species differences between protein and/or test animal.

Table 2
Percent changes of half-life and organ uptake clearances of HSA variants in mice

Variant name (mutation)	Half-life (%)	Liver clearance (%)	Kidney clearance (%)	Spleen clearance (%)	α-helical content (%)	ΔH_v[a] (%)
proAlb Lille (−2Arg->His)	−4.99	31.58	−24.63	−8.48	−9.60	−6.08
proAlb Tradate (−2Arg->Cys)	−1.19	1.82	93.74	−14.84	−24.15	N.D.[b]
Arg-Alb (Alb A having −1 Arg)	3.39	−77.58	−16.25	15.75	5.64	3.80
Alb Bazzano (567–582 substituted, 583–585 deleted)	−5.73	358.94	111.49	46.10	−20.09	−4.49
Alb Venezia (572–578 substituted, 579–585 deleted)	−8.94	225.74	116.50	30.32	5.41	34.50
Alb Catania (580–582 substituted, 583–585 deleted)	−1.07	−74.92	71.83	−12.75	−1.09	−19.71
Alb Malmö-95 (63 Asp->Asn, glycosylated at 63 Asn)	−1.10	82.91	2.07	−35.65	−0.31	−30.75
Alb Redhill (−1 Arg retained, 320 Ala->Thr, glycosylated at 318 Asn)	6.16	−72.52	−50.24	−45.63	−3.26	−4.48
Alb Casebrook (494 Asp->Asn, glycosylated at 494 Asn)	0.84	65.49	−5.17	−1.36	−7.06	17.54

[a] The values for ΔH_v are taken from Kragh-Hansen et al. [15].
[b] ND, Not determined.

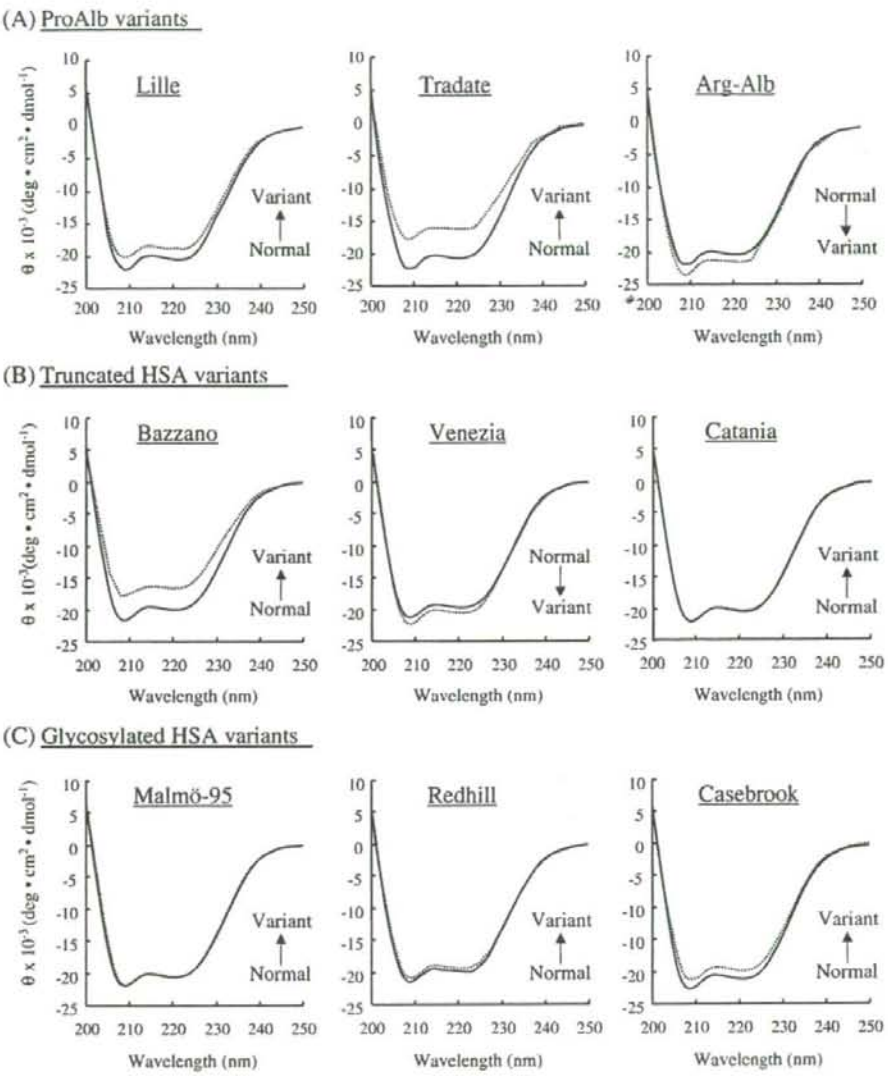

Fig. 3. Far-UV CD spectra of proAlb variants (A), truncated HSA variants (B) and glycosylated HSA variants (C) and their corresponding Alb A. The dotted and full curves represent variant and normal albumin, respectively. The curves are averages for three experiments.

In addition to change in chain-length and glycosylation we investigated whether the modified plasma half-lives could be correlated to other molecular parameters. Therefore, we estimated the effect of genetic variation on the α-helical content of albumin and related any changes to the changes in plasma half-life and organ uptakes. However, no clear correlation could be found between the changes in α-helical content and the different pharmacokinetic parameters (not shown). The changes in half-life and organ uptakes were also compared to mutation-induced changes in heat stability; quantified by using ΔH_v [15]. However, also in this case no correlations were found (not shown).

For being able to explain, at least in part, the modified plasma half-lives of the genetic variants we investigated their liver, kidney and spleen uptake clearances (Table 1). The diminished plasma half-lives of Alb Bazzano and Venezia are in full accordance with pronounced increases in liver, kidney and spleen uptake clearances. Likewise, the increased half-life of Alb Redhill can fully, or partly, be caused by diminished uptake by the three organs. Although most of the remaining variants have an increased liver clearance and a reduced spleen uptake individual results were obtained for these six alloalbumins. However, for all variants also other metabolic factors could be modified, see below.

Uptake of HSA by liver, kidney and spleen is mainly due to the presence of cell membrane receptors which recognize the protein and then internalize it by endocytosis. Some of these receptors interact with native protein, whereas other receptors interact with modified protein, and both types of interactions could be affected by genetic variation of albumin. Thus, binding of HSA to the membrane-bound receptor gp60 initiating a transcellular pathway for albumin across the endothelial cell wall to the underlying interstitium [34] could be affected. Sometimes, a glycosylated albumin variant looses one or both of the sialic acid residues on the antennae. Since the remaining of

the glycans has galactose and mannose units, these forms could interact with increased affinity with the galactosyl receptor-mediated (asialoglycoprotein receptor-mediated) endocytotic pathway of the hepatocytes and the mannose receptor-mediated endocytotic pathway of non-parenchymal cells in the liver. The liver also possesses receptors for rapid uptake of oxidized albumin and albumin with advanced glycation end products. Whether the present molecular changes can initiate endocytosis by scavenger receptors such as gp18, gp30, stabilin-1 or stabilin-2 is at present only speculative. However, liver uptake by adsorptive endocytosis could be influenced by the molecular changes, because this type of uptake is dependent on the net charge of the protein.

Normally, glomerular filtration of HSA in the kidneys is followed by its return into the venous circulation without degradation (the albumin retrieval pathway). However, part of the protein reabsorbed by the proximal tubule cells, most probably via the endocytic receptors megalin and cubulin, is degradated in the lysosomes. Whether genetic modification of HSA affects glomerular filtration and/or reabsorbtion of the protein remains to be clarified. However, since the size and charge of albumin influence glomerular filtration, especially the glycosylated variants could have an altered handling by the glomeruli. It should be noted that no radioactivity was detected in the urine during the present experimental period. An alternative, or supplementary, explanation for the modified uptake of the albumin isoforms by the kidney could be the presence of tubular RAGE which is known to cause the internalization of proteins with advanced glycation end products. Irrespective of the detailed mechanism, the net effect of deleting three or more C-terminal amino acids is an increased kidney uptake clearance (Tables 1 and 2). The effect of glycosylation depends on the position of attachment, because glycosylation of domain II (Alb Redhill) decreases uptake, whereas glycosylation of domain I (Alb Malmö-95) and domain III (Alb Casebrook) has no significant effect on kidney uptake.

Glycosylation diminishes uptake by the spleen (Tables 1 and 2). This is most evident for Alb Redhill, especially when taking into account that the presence of −1 Arg increases uptake. The presence of a modified propeptide also decreases clearance uptake. By contrast, the truncated variants with the most pronounced molecular changes (Alb Bazzano and Venezia) have significantly increased uptakes. Apparently, less is known about endocytosis-associated membrane receptors in the spleen than in the liver and kidneys. However, the organ most probably also has endothelial cells with the receptor gp60 [34]. In addition, it harbors scavenger receptors such as stabilin-1 and stabilin-2. To what extent albumin-receptor interactions are affected by the mutations remains to be elucidated.

More recently, another type of endocytosis of HSA has been identified in virtually all nucleated cells which results in reuse of the protein [35–37]. After pinocytosis, albumin binds intracellularly and in a pH-dependent manner to the receptor FcRn. Thereby the protein is diverted from the lysosomal degradation pathway and exocytosed back to the circulation in an intact form extending its plasma half-life. Anderson et al. [35] have proposed that the intracellular binding of HSA to FcRn is due to a hydrophobic interaction, whereas Chaudhury et al. [36] suggested interaction(s) between histidine residue(s) in the receptor and histidine residues in domain III of albumin. By contrast, Andersen et al. [37] suggested that FcRn interacts with negatively charged and surface exposed residues on domain III of HSA. However, the authors cited agree that domain III of albumin seems to contain all of the FcRn binding activity, why especially genetic variants with domain III changes could have modified plasma half-lives due to a modified HSA–FcRn recycling process.

The metabolism of HSA can be affected by enzymes such as aminopeptidase(s) and carboxypeptidase(s) in the circulation. That has been observed in, for example, a patient with a severe traumatic injury, who had an increased activity of carboxypeptidase A resulting in hydrolysis of the C-terminal leucine and a fast elimination of albumin from the blood: the half-life was changed from ca. 19 days to less than 80 h [38]. In addition, modified albumin can be a substrate for endopeptidase(s) in the blood. Thus, oxidized bovine serum albumin, but not the native protein, can be cleaved by oxidized protein hydrolase [39]. Because the hydrolase is found in the blood, also this enzyme could hydrolyse some of the genetic variants in the mouse circulation and thereby render them more exposed to organ uptake.

In conclusion, the pharmacokinetics of HSA can be modified by changes in chain-length and by glycosylation. Three of the alloalbumins with a modified chain-length had a significantly shorter half-life in the circulation, whereas a glycosylated protein had an increased half-life (Table 1). These findings are useful when trying to construct an isoform with a modified stability in plasma. If an isoform with a shorter half-life is wanted, it is probably preferable to choose one with a C-terminally shortened chain-length rather than one with a N-terminally elongated chain-length, because the presence of a propeptide is known to block the high-affinity binding site for metal ions such as Cu^{++} and Ni^{++} [40]. It is a disadvantage to block this binding site, because albumin binding of Cu^{++} is an element in our anti-oxidative defense. Liver, kidney and spleen clearances were determined, and eight of the nine genetic variants had one or more modified organ uptakes. The uptakes measured are net effects of organ uptake leading to destruction in the lysosomes or to recycling via the FcRn receptor. The uptakes themselves and the two intracellular pathways could be affected differently by the protein modifications. The results revealed that if an increased uptake in the three organs is wanted for, for example, drug delivery systems, then truncated variants like Alb Bazzano and Venezia are good candidates. If the opposite is wanted, namely decreased uptakes in the organs, then the glycosylated Alb Redhill could be useful. Finally, we investigated whether blood half-lives or organ uptakes are directly related to mutation-induced changes in the proteins α-helical content or to changes in ΔH_m representing thermal stability. However, that was found not to be the case.

Acknowledgements

This work was supported, in part, by Grants-in-Aid for Scientific Research from the Ministry of Education, Science, Sports and Culture of Japan (14370759) and by Fonden af 1870.

References

[1] U. Kragh-Hansen, Molecular aspects of ligand binding to serum albumin, Pharmacol. Rev. 33 (1981) 17–53.
[2] T. Peters Jr., All About Albumin: Biochemistry, Genetics, and Medical Applications, Academic Press, San Diego, CA, 1996.
[3] D.C. Carter, J.X. Ho, Structure of serum albumin, Adv. Protein Chem. 45 (1994) 153–203.
[4] S. Sugio, A. Kashima, S. Mochizuki, M. Noda, K. Kobayashi, Crystal structure of human serum albumin at 2.5 A resolution, Protein Eng. 12 (1999) 439–446.
[5] M.L. Ferrer, R. Duchowicz, B. Carrasco, J.G. de la Torre, A.U. Acuna, The conformation of serum albumin in solution: a combined phosphorescence depolarization-hydrodynamic modeling study, Biophys. J. 80 (2001) 2422–2430.
[6] K. Kobayashi, Summary of recombinant human serum albumin development, Biologicals 34 (2006) 55–59.
[7] S. Matsushita, V.T.G. Chuang, M. Kanazawa, S. Tanase, K. Kawai, T. Maruyama, A. Suenaga, M. Otagiri, Recombinant human serum albumin dimer has high blood circulation activity and low vascular permeability in comparison with native human serum albumin, Pharm. Res. 23 (2006) 882–891.
[8] T. Komatsu, Y. Oguro, Y. Teramura, S. Takeoka, J. Okai, M. Anraku, M. Otagiri, E. Tsuchida, Physicochemical characterization of cross-linked human serum albumin dimer and its synthetic heme hybrid as an oxygen carrier, Biochim. Biophys. Acta 1675 (2004) 21–31.
[9] W.P. Sheffield, J.A. Marques, V. Bhakta, I.J. Smith, Modulation of clearance of recombinant serum albumin by either glycosylation or truncation, Thromb. Res. 99 (2000) 613–621.
[10] G.M. Subramanian, P.A. Moore, B.B. Gowen, A.L. Olsen, D.L. Barnard, J. Paragas, R.J. Hogan, R.W. Sidwell, Potent in vitro activity of the albumin fusion type I interferons (albumin-interferon-alpha and albumin-interferon-beta) against RNA viral agents of bioterrorism and the severe acute respiratory syndrome (SARS) virus, Chemotherapy 54 (2008) 176–180.

[11] J. Chen, G. Bai, Y. Cao, Z. Gao, Q. Zhang, Y. Zhu, W. Yang, One-step purification of a fusion protein of glucagon-like peptide-1 and human serum albumin expressed in *Pichia pastoris* by an immunomagnetic separation technique, Biosci. Biotechnol. Biochem. 71 (2007) 2655–2662.
[12] R.J. Melder, B.L. Osborn, T. Riccobene, P. Kanakaraj, P. Wei, G. Chen, D. Stolow, W.G. Halpern, T.-S. Migone, Q. Wang, K.J. Grzegorzewski, G. Gallant, Pharmacokinetics and in vitro and in vivo anti-tumor response of an interleukin-2-human serum albumin fusion protein in mice, Cancer Immunol. Immunother. 54 (2005) 535–547.
[13] L. Minchiotti, M. Galliano, U. Kragh-Hansen, T. Peters Jr., Mutations and polymorphisms of the gene of the major human blood protein, serum albumin, Hum. Mutat. 29 (2008) 1007–1016.
[14] Y. Iwao, M. Hiraike, U. Kragh-Hansen, K. Mera, T. Noguchi, M. Anraku, K. Kawai, T. Maruyama, M. Otagiri, Changes of net charge and α-helical content affect the pharmacokinetic properties of human serum albumin, Biochim. Biophys. Acta 1774 (2007) 1582–1590.
[15] U. Kragh-Hansen, S. Saito, K. Nishi, M. Anraku, M. Otagiri, Effect of genetic variation on the thermal stability of human serum albumin, Biochim. Biophys. Acta 1747 (2005) 81–88.
[16] U. Kragh-Hansen, A micromethod for delipidation of aqueous proteins, Anal. Biochem. 210 (1993) 318–327.
[17] R.F. Chen, Removal of fatty acids from serum albumin by charcoal treatment, J. Biol. Chem. 242 (1967) 173–181.
[18] D.J. Hnatowich, W.W. Layne, R.L. Childs, The preparation and labelling of DTPA-coupled albumin, Int. J. Appl. Radiat. Isot. 33 (1982) 327–332.
[19] F. Staud, M. Nishikawa, K. Morimoto, Y. Takakura, M. Hashida, Disposition of radioactivity after injection of liver-targeted proteins labeled with 111In or 125I. Effect of labeling on distribution and excretion of radioactivity in rats, J. Pharm. Sci. 88 (1999) 577–585.
[20] J.R. Duncan, M.J. Welch, Intracellular metabolism of indium-111-DTPA-labeled receptor targeted proteins, J. Nucl. Med. 34 (1993) 1728–1738.
[21] K. Yamaoka, Y. Tanigawara, T. Nakagawa, T. Uno, A pharmacokinetic analysis program (multi) for microcomputer, J. Pharmacobio-Dyn. 4 (1981) 879–885.
[22] M.M. Bradford, A rapid and sensitive method for the quantitation of microgram quantities of protein utilizing the principle of protein-dye binding, Anal. Biochem. 72 (1976) 248–254.
[23] Y.-H. Chen, J.T. Yang, H.M. Martinez, Determination of the secondary structures of proteins by circular dichroism and optical rotatory dispersion, Biochemistry 11 (1972) 4120–4131.
[24] Y. Abdo, J. Rousseaux, M. Dautrevaux, Proalbumin Lille, a new variant of human seum albumin, FEBS Lett. 131 (1981) 286–288.
[25] S.O. Brennan, K. Arai, J. Madison, C.-B. Laurell, M. Galliano, S. Watkins, R. Peach, T. Myles, P. George, F.W. Putnam, Hypermutability of CpG dinucleotides in the propeptide-encoding sequence of the human albumin gene, Proc. Natl. Acad. Sci. U. S. A. 87 (1990) 3909–3913.
[26] S. Watkins, J. Madison, E. Davis, Y. Sakamoto, M. Galliano, L. Minchiotti, F.W. Putnam, A donor splice mutation and a single-base deletion produce two carboxylterminal variants of human serum albumin, Proc. Natl. Acad. Sci. U. S. A. 88 (1991) 5959–5963.
[27] J. Madison, M. Galliano, S. Watkins, L. Minchiotti, F. Porta, A. Rossi, F.W. Putnam, Genetic variants of human serum albumin in Italy: point mutants and a carboxyl-terminal variant, Proc. Natl. Acad. Sci. U. S. A. 91 (1994) 6476–6480.
[28] Y. Sakamoto, K. Kitamura, J. Madison, S. Watkins, C.-B. Laurell, M. Nomura, T. Higashiyama, F.W. Putnam, Structural study of the glycosylated and unglycosylated forms of a genetic variant of human serum albumin (63 Asp→Asn), Biochim. Biophys. Acta 1252 (1995) 209–216.
[29] S.O. Brennan, T. Myles, R.J. Peach, D. Donaldson, P.M. George, Albumin Redhill (−1 Arg, 320 Ala→Thr): a glycoprotein variant of human serum albumin whose precursor has an aberrant signal peptidase cleavage site, Proc. Natl. Acad. Sci. U. S. A. 87 (1990) 26–30.
[30] U. Kragh-Hansen, D. Donaldson, P.H. Jensen, The glycan structure of albumin Redhill, a glycosylated variant of human serum albumin, Biochim. Biophys. Acta 1550 (2001) 20–26.
[31] R.J. Peach, S.O. Brennan, Structural characterization of a glycoprotein variant of human serum albumin: albumin Casebrook (494 Asp→Asn), Biochim. Biophys. Acta 1097 (1991) 49–54.
[32] P.A. Haynes, M. Batley, R.J. Peach, S.O. Brennan, J.W. Redmond, Characterization of oligosaccharides from a glycoprotein variant of human serum albumin (albumin Casebrook) using high-performance anion-exchange chromatography and nuclear magnetic resonance spectroscopy, J. Chromatogr. 581 (1992) 187–193.
[33] S.O. Brennan, A.P. Fellowes, Albumin Hawkes Bay: a low level variant caused by loss of a sulphydryl group at position 177, Biochim. Biophys. Acta 1182 (1993) 46–50.
[34] T.A. John, S.M. Vogel, C. Tiruppathi, A.B. Malik, R.D. Minshall, Quantitative analysis of albumin uptake and transport in the rat microvessel endothelial monolayer, Am. J. Physiol., Lung Cell Mol. Physiol. 284 (2003) L187–L196.
[35] C.L. Anderson, C. Chaudhury, J. Kim, C.L. Bronson, M.A. Wani, S. Mohanty, Perspective - FcRn transports albumin: relevance to immunology and medicine, Trends Immunol. 27 (2006) 343–348.
[36] C. Chaudhury, C.L. Brooks, D.C. Carter, J.M. Robinson, C.L. Anderson, Albumin binding to FcRn: distinct from the FcRn–IgG interaction, Biochemistry 45 (2006) 4983–4990.
[37] J.T. Andersen, J.D. Qian, I. Sandlie, The conserved histidine 166 residue of the human neonatal Fc receptor heavy chain is critical for the pH-dependent binding to albumin, Eur. J. Immunol. 36 (2006) 3044–3051.
[38] D. Bar-Or, L.T. Rael, R. Bar-Or, D.S. Slone, M.L. Craun, The formation and rapid clearance of a truncated albumin species in a critically ill patient, Clin. Chim. Acta 365 (2006) 346–349.
[39] T. Fujino, M. Kojima, M. Beppu, K. Kikugawa, H. Yasuda, K. Takahashi, Identification of the cleavage sites of oxidized protein that are susceptible to oxidized protein hydrolase (OPH) in the primary and tertiary structures of the protein, J. Biochem. 127 (2000) 1087–1093.
[40] U. Kragh-Hansen, S.O. Brennan, L. Minchiotti, M. Galliano, Modified high-affinity binding of Ni^{2+}, Ca^{2+} and Zn^{2+} to natural mutants of human serum albumin and proalbumin, Biochem. J. 301 (1994) 217–223.

Biochimica et Biophysica Acta 1784 (2008) 1441–1447

Contents lists available at ScienceDirect

Biochimica et Biophysica Acta

journal homepage: www.elsevier.com/locate/bbapap

NO and CO binding profiles of hemoglobin vesicles as artificial oxygen carriers

Hiromi Sakai [a], Atsushi Sato [b], Peter Sobolewski [c,d], Shinji Takeoka [b], John A. Frangos [c], Koichi Kobayashi [e], Marcos Intaglietta [c,d], Eishun Tsuchida [a,*]

[a] Research Institute for Science and Engineering, Waseda University, Tokyo 169-8555, Japan
[b] Graduate School of Science and Engineering, Waseda University, Tokyo 169-8555, Japan
[c] La Jolla Bioengineering Institute, La Jolla, CA 92037, USA
[d] Department of Bioengineering, University of California, San Diego, La Jolla, CA 92093-0412, USA
[e] Department of Surgery, School of Medicine, Keio University, Tokyo 160-8582, Japan

ARTICLE INFO

Article history:
Received 27 November 2007
Received in revised form 16 February 2008
Accepted 10 March 2008
Available online 20 March 2008

Keywords:
Blood substitutes
Artificial red cells
Liposome
NO
CO
Vasoconstriction

ABSTRACT

Hemoglobin vesicles (HbVs) are artificial oxygen carriers encapsulating purified and concentrated Hb solution in phospholipid vesicles (liposomes). We examined in-vitro reaction profiles of a formulation of HbV with NO and CO in anaerobic and aerobic conditions using stopped-flow spectrophotometry and a NO electrode. Reaction rate constants of NO to deoxygenated and oxygenated HbV were considerably smaller than those of cell-free Hb because of the intracellular NO-diffusion barrier. The reaction of CO with deoxygenated HbV was slightly slower than that of cell-free Hb solely because of the co-encapsulated allosteric effector, pyridoxal 5'-phosphate. The NO depletion in an aerobic condition in the presence of empty vesicles was monitored using a NO electrode, showing that the hydrophobic bilayer membrane of HbV, which might have higher gas solubility, does not markedly facilitate the O_2 and NO reaction, and that the intracellular Hb is the major component of NO depletion. In conclusion, HbV shows retarded gas reactions, providing some useful information to explain the absence of vasoconstriction and hypertension when they are intravenously injected.

1. Introduction

A physiologically important aspect of the structure of red blood cells (RBCs) is the management of the transport of endogenous gaseous messenger molecules (NO and CO) [1–3]. Conditions of hemolysis [4] and studies related to the development of hemoglobin-based oxygen carriers (HBOCs) [5–11] have shown that the entrapment of endothelium-derived NO induces vasoconstriction, hypertension, reduced blood flow, and vascular damage. Physiological doses of CO are a vasorelaxation factor, especially in the hepatic microcirculation [12] and its entrapment by cell-free hemoglobin (Hb) solutions induces constriction of sinusoidal capillaries [13]. These side effects due to the presence of molecular Hb in plasma suggest that the cellular structure of RBCs plays a role in insuring the bioavailability of NO and CO.

Several mechanism have been proposed to explain NO binding retardation by Hb encapsulation in RBCs [14–16], namely: (i) an unstirred layer forming an extracellular diffusion barrier surrounding the RBC [2,14]; (ii) a protein-rich RBC cytoskeletal submembrane constituting a physical barrier against NO diffusion [17,18]; and (iii) retardation of gas diffusion due to the viscosity of the Hb solution in RBCs [19].

Hemoglobin has been encapsulated using lipid bilayer membranes to form Hb vesicles (HbV), in order to produce a blood like HBOC where the oxygen carrying Hb is not dissolved in plasma [20,21]. In this configuration Hb is not vasoactive [9,10], an effect in part due to the retardation of NO binding by Hb encapsulation in phospholipid vesicles [22]. Furthermore, using results of stopped-flow spectrophotometry and computer simulation, we recently determined that the major component of retardation is the intracellular rather than the extracellular diffusion barrier. This conclusion is also supported by considering that: (i) the large binding rate constant of NO to a heme in an Hb molecule, (ii) the numerous hemes as sites of gas entrapment at a high intracellular Hb concentration $[Hb]_{in}$, (iii) the slowed gas diffusion in the intracellular viscous Hb solution; and (iv) the lipid bilayer membrane of HbV would not possess any barrier function to the NO diffusion into the particles [23].

On the other hand, the hydrophobic part of a cell membrane reportedly possesses higher gas solubility than the bulk aqueous phase. Both NO and O_2 dissolve to a greater extent in the hydrophobic part, which facilitates the reaction of NO with O_2 to produce NO_3^- [24]. HbV mimics the structure of RBCs, however the particle diameter is much smaller than that of RBCs, and the surface to volume ratio is larger. Therefore for the same oxygen carrying capacity, or equivalent cell concentration by volume there is proportionally greater amount of membrane material for HbVs than for RBCs providing a greater

Abbreviations: HbV, hemoglobin vesicles; RBC, red blood cells; $k'^{(NO)}_{on}$, apparent NO binding rate constant; $k'^{(CO)}_{on}$, apparent CO binding rate constant; $k'^{(NO)}_{ox}$, apparent oxidation rate by NO; PLP, pyridoxal 5'-phosphate; DPPC, 1,2-dipalmitoyl-sn-glycero-3-phosphatidylcholine

* Corresponding author. Tel.: +81 3 5286 3120; fax: +81 3 3205 4740.
E-mail address: eishun@waseda.jp (E. Tsuchida).

1570-9639/$ – see front matter © 2008 Elsevier B.V. All rights reserved.
doi:10.1016/j.bbapap.2008.03.007

hydrophobic domain. This structural difference is important because it is likely that there is NO depletion in the lipid bilayer membrane of HbVs.

In the present study we analyzed the NO and CO binding rates of HbV with the present formulation, along with the possibility of accelerated NO depletion in the hydrophobic domain of the HbV lipid bilayer membrane. We compared our findings to the corresponding binding rates of a purified human Hb solution suspended in phosphate buffered saline solution (PBS) mixed with pyridoxal 5'-phosphjate (PLP), a solution of polymerized bovine Hb (poly$_B$Hb) used for veterinary purposes (Oxyglobin; Biopure Corp. Cambridge, MA) [25], and vesicles containing saline solution.

2. Materials and methods

2.1. Hb vesicles (HbV), Hb solutions, empty vesicles (EV), and RBCs

HbVs were prepared as reported previously [26–29], with slight modifications. Human Hb solution was obtained through purification of outdated RBCs provided by the Japanese Red Cross Society (Tokyo, Japan). Hb was stabilized by carbonylation (HbCO) and concentrated by ultrafiltration to 38 g/dL. PLP (Sigma, St. Louis, MO) was added to the HbCO solution as an allosteric effector at a molar ratio of PLP/Hb tetramer=2.5. We use PLP instead of 2,3-diphosphoglyceric acid (2,3-DPG) or inositol hexaphosphate (IHP) because 2,3-DPG is very unstable and expensive, and the interaction of IHP and Hb is so strong that the oxygen dissociation curve of Hb is distorted and the Hill number becomes nearly 1 [30].

The Hb solution with PLP was then mixed with lipids and encapsulated in vesicles. The lipid bilayer was comprised of 1,2-dipalmitoyl-*sn*-glycero-3-phosphatidylcholine (DPPC), cholesterol, 1,5-*O*-dihexadecyl-*N*-succinyl-L-glutamate (Nippon Fine Chemical Co. Ltd., Osaka, Japan), and 1,2-distearoyl-*sn*-glycerol-3-phosphatidylethanolamine-*N*-PEG$_{5000}$ (DSPE-PEG; NOF Corp., Tokyo, Japan) at a molar composition of 5/5/1/0.033. Particle diameter was regulated by extrusion. The encapsulated HbCO was converted to HbO_2 by exposing the liquid membrane of HbV to visible light under an O_2 atmosphere. The particle size distribution was measured using a light-scattering method (Submicron Particle Size Analyzer, model N4 PLUS; Beckman-Coulter, Inc., Fullerton, CA). An empty vesicle (EV) suspension was prepared using the same lipids through hydration with a saline solution. The lipid concentration (6.8 g/dL) and the particle diameter (ca. 250 nm) were almost identical to those of HbV.

A purified human Hb solution suspended in phosphate buffered saline solution (PBS) was prepared and mixed with PLP at molar ratios of PLP/Hb tetramer=0 and 2.5. We also used the polymerized bovine Hb solution (poly$_B$Hb) (Oxyglobin; Biopure Corp. Cambridge, MA) [25]. This solution is a mixture of nonpolymerized tetrameric $_B$Hb (37.2%) and polymerized $_B$Hb with a wide molecular weight distribution [25]. The P_{50} values and Hill numbers of HbV and Hb solutions were obtained from the oxygen equilibrium curve measured using a Hemox-Analyzer (TCS Medical Science, Philadelphia, PA) at 37 °C [23,31] (Fig. 1).

Blood was harvested from female C57BL/129 mice in accordance with IACUC protocol. RBCs were pelleted at 800 g for 30 min and resuspended and washed twice with a 40 mM-HEPES buffer (pH=7.4, 5 mM glucose, Sigma, St. Louis, MO; tonicity, 285 mOms regulated with NaCl). The RBC suspensions were prepared at a concentration of 2×10^6 cells/mL ([Hb]=0.93 μM, [heme]=3.72 μM) in the same HEPES buffer.

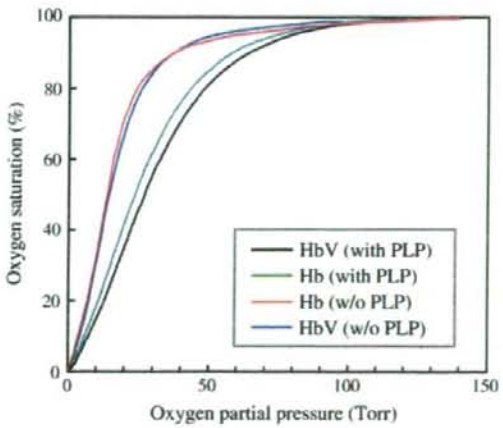

Fig. 1. Oxygen dissociation curves of Hb solutions and HbV with or without PLP measured with Hemox-Analyzer at 37 °C. The P_{50} values and Hill numbers are listed in Table 1. The data of HbV (w/o PLP) is cited from our previous study [23].

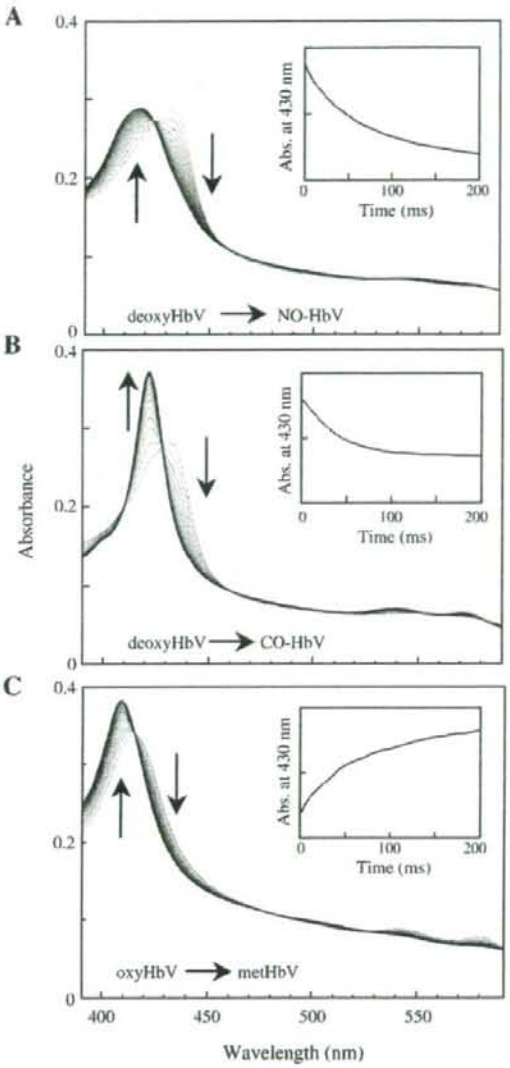

Fig. 2. Representative profiles of the reactions of NO or CO-HbV using stopped-flow spectrophotometry. (A) A NO-bubbled PBS ([NO]=3.8 μM) and deoxygenated HbV in PBS ([heme]=3.0 μM) were mixed rapidly; the absorption spectra were collected every millisecond for 0.2 s after mixing. In this figure, the spectroscopic curves of every 10 ms are selected. The figure shows clearly that the spectrum of deoxyHbV is mostly converted to NO-HbV during 0.2 s. (inset) The time course of the measured absorbance at 430 nm. (B) A CO-bubbled PBS ([CO]=135 μM) and deoxygenated HbV in PBS ([heme]=3.0 μM) were mixed rapidly using a stopped-flow spectrophotometer. This figure clearly shows that the spectrum of deoxyHbV is mostly converted to CO-HbV in 0.2 s. (inset) The time course of the measured absorbance at 430 nm. (C) A NO-bubbled PBS ([NO]=3.8 μM) and oxygenated HbV in PBS ([heme]=3.0 μM) were mixed. The spectrum of oxygenated HbV is mostly converted to metHbV during 0.2 s. (inset) The time course of the measured absorbance at 408 nm. The optical path length was 1 cm. In these experimental conditions, the CO binding in (C) seems faster than the NO reactions (A and B), due to the higher concentration of CO (135 μM) than that of NO (3.8 μM). However, the calculated reaction rate constant of the CO binding is much smaller than those of NO reactions as shown in Table 1.

2.2. Stopped-flow spectrophotometry

The time course of the ligand binding was analyzed during rapid mixing of the deoxygenated HbV and Hb solutions and a NO- or CO-containing solution using a stopped-flow rapid scan spectrophotometer (RSP-1000; Unisoku Co. Ltd., Osaka, Japan)

[22,23]. Solutions in the two gas-tight reservoirs (A and B) are mixed rapidly applying a pressure of 0.3–0.6 MPa; the dead time for mixing being < 1.5 ms. All measurements were performed at 25 °C. A PBS solution (3 ml each) was poured into both reservoirs, which were both sealed using septum rubber seals. The reservoirs were deoxygenated by N_2 bubbling for more than 30 min. A stock solution of HbV or Hb (ca. 30 μl, [heme]≈300 μM) was injected into Reservoir A to adjust [heme] to 3 μM and the N_2 bubbling was changed to a flow to avoid denaturation of the solutes. Complete deoxygenation was confirmed using preliminary stopped-flow measurements (wavelength: 385–593 nm), where the Soret band showed a maximum absorbance (λ_{max}) at 430 nm because of the presence of deoxyHb. To make the reservoirs deoxygenated, we did not use sodium dithionate because it is well known that an excess amount of this reagent sometimes possibly induces chemical modifications of heme or globin [32,33]. In Reservoir B, NO or CO gas bubbling was started while a gentle N_2 flow was maintained in Reservoir A. The mixed gases for NO binding (NO, 0.2029%; N_2, 99.7971%) and for CO binding (CO, 14.14%; N_2, 85.86%) were purchased from Takachiho Chemical Industrial Co., Ltd. (Tokyo).

Stopped-flow measurement was initiated after about 10 min bubbling. The sampling interval and the exposure time were set as 1 ms and measurement time was 210 ms. All measurements were performed 3 times and the change of absorbance at 430 nm was plotted as a function of time. The apparent binding rate constants of NO and CO ($k'^{(NO)}_{on}$ and $k'^{(CO)}_{on}$, respectively) were calculated using Eq. (1) under the assumption of homogeneous distribution of Hb, irreversible second order reaction, and a pseudo-first order reaction when gas molecules are abundant.

$$\ln\frac{\Delta A_t}{\Delta A_0} = -k'_{on}\cdot C_{Gas}\cdot t. \quad (1)$$

In this equation, ΔA_t is the change of absorbance at 430 nm at time t ($=A_t-A_{t=\infty}$) and A_0 is the absorbance at the initial time ($=A_{t=0}-A_{t=\infty}$), and C_{Gas} is the initial gas concentration. NO (1.9 μM) was not much more abundant than the heme concentration (1.5 μM) in the NO-reaction experiments, therefore the apparent binding rates were calculated from the slopes of the initial phase of reactions. The time courses of the reaction of NO and O_2-bound HbV or HbO_2 solutions were analyzed using stopped-flow spectrometry in the same manner, except that an air-equilibrated PBS solution was introduced into Reservoir A to ensure the O_2-binding state. The absorption changes were monitored at 408 nm.

2.3. Measurement of NO depletion using a NO electrode

The rate of NO depletion in a test solution after adding NO in an aerobic condition was monitored via an amino-700 probe and an inNO-T sensor (Innovative Instruments, Inc.) connected to a Dell PC running InNO-T software (Innovative Instruments, Inc.) [34]. In a room atmosphere, 3 mL of a PBS solution containing HbV, EV, or mice RBCs was pipetted into a cuvette and stirred using a magnetic stir bar. The NO sensor was introduced into the cuvette for continuous monitoring. After a steady condition was confirmed, a stock NO solution (100 μL) was injected, yielding the concentration of 2 μM NO. The NO level rapidly increases and then decreases with the reaction with O_2 and Hb. Concentrations of the specimens were as follows: HbV ([heme]=4 μM, [Hb]=65 mg/L, [Lipid]=36 mg/L), EV ([lipid]=36 mg/L), and mice RBC ([heme]=3.72 μM). Data were fitted and basic statistics and graphs were obtained using Synergy KaleidaGraph 3.6. Correlation was determined using Spearman's rank correlation test, with StatView 5.

3. Results

3.1. Stopped-flow spectrophotometry of NO and CO bindings in an anaerobic condition

Complete deoxygenation of HbV was confirmed using the characteristic wavelength of the maximum absorption (λ_{max}) at 430 nm. Because of the stronger light-scattering effect of the HbV suspension than that of the Hb solution and RBCs [35], the absorption peaks in the Q band region were not well defined in this measurement. After rapid mixing with NO, the immediate absorption reduction at 430 nm and the increase at 418 nm that correspond to the formation of HbNO were confirmed (Fig. 2A). In the case of mixing with CO, the immediate absorption increase at 419 nm was confirmed (Fig. 2B). The change of absorption at 430 nm in both reactions was indicative of the formation of HbNO or HbCO in the vesicles.

The spectrophotometric scans presented in Fig. 2A and B were performed 3 times and the averaged level of reaction was plotted as a ratio of absorbance at 430 nm (A_t) at time t, to the initial absorbance (ΔA_0) at time 0 (Fig. 3A and B). Data of Hb solutions are also plotted in those figures. The graph clearly shows that both NO binding and CO binding were slower for HbV than for the human Hb solution without PLP. However, Hb with PLP showed almost identical CO binding to HbV. The NO binding rates of Hb solution with and without PLP and $poly_BHb$ were almost identical. The apparent binding rate constants of $k'^{(NO)}_{on}$ for NO and $k'^{(CO)}_{on}$ for CO are presented in Table 1.

3.2. Stopped-flow spectrophotometry of the reaction of NO and O_2-bound HbV and Hb solutions in an aerobic condition

The oxygenated HbV showed the absorption maximum at 415 nm (Fig. 2C). Mixing with NO showed the immediate reduction of the absorption maximum, although an increase at 405 nm showed attributes of the metHb formation. The spectrophotometry scans portrayed in Fig. 2C were performed 3 times and the average level of reaction was plotted as a ratio of absorbance at 408 nm ($\Delta A_t=A_t-A_{t=\infty}$) at time t, to the initial absorbance ($\Delta A_0=A_{t=0}-A_{t=\infty}$) at time 0 (Fig. 3C).

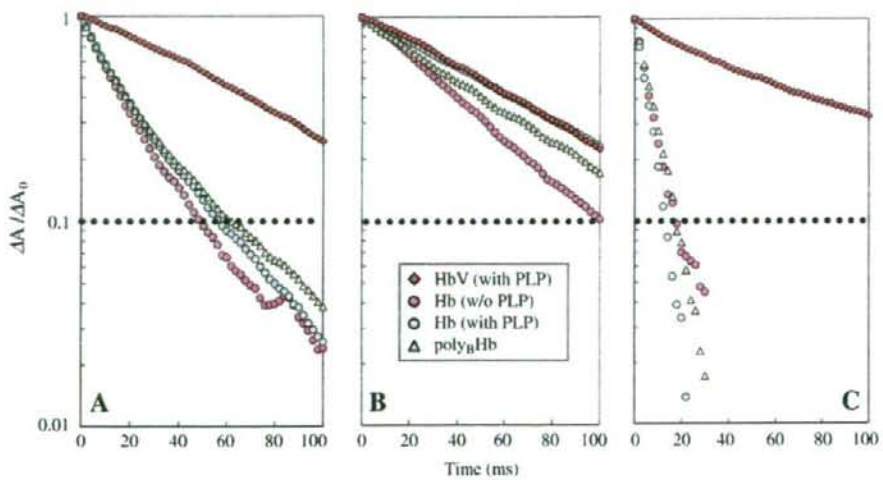

Fig. 3. Time courses of NO and CO reactions by Hb V, human Hb solutions, and $Poly_BHb$. The level of reaction was plotted on a semi-logarithmic graph as a ratio of absorption at 419 or 430 nm (ΔA_t) at time t, to the initial absorption (A_0) at time 0. (A) A NO-bubbled PBS ([NO]=3.8 μM) and deoxygenated-Hb-containing solutions in PBS ([heme]=3.0 μM) were mixed. (B) A CO-bubbled PBS ([CO]=135 μM) and deoxygenated-Hb-containing solutions in PBS ([heme]=3.0 μM) were mixed. (C) A NO-bubbled PBS ([NO]=3.8 μM) and an oxygenated-HbO_2-containing solution in PBS ([heme]=3.0 μM) were mixed.

Table 1
Apparent reaction rate constants of Hb, HbV, and polyHb with different P_{50}. The data of HbV without PLP were referred from a previous paper [23]

	HbV (with PLP)	HbV[a] (w/o PLP)	Hb (with PLP)	Hb (w/o PLP)	$poly_BHb$
$k_{on}^{(CO)}$ (10^5 M^{-1} s^{-1})	2.1	3.4[a]	2.1	3.4	2.7
$k_{on}^{(NO)}$ (10^7 $M^{-1}s^{-1}$)	0.61	0.88[a]	2.4	2.6	2.4
$k_{on}^{(O2)}$ (10^7 $M^{-1}s^{-1}$)	0.88	–	8.7	7.4	6.6
P_{50} (Torr)	25–31	14[a]	23	14	54[b]
Hill number	2.1	2.1	1.9	2.2	1.2[b]
Size	279 nm	265 nm[a]	65 kDa	65 kDa	87–502 kDa[c]

[a] Reference [23].
[b] Reference [31].
[c] Reference [25].

The graph shows that the reaction of NO with oxygenated HbV was considerably slower than that of human Hb solutions with and without PLP. The rate of $poly_BHb$ was almost identical to that of human Hb solutions. The apparent oxidation reaction rate constants $k^{(NO)}$ are summarized in Table 1.

3.3. NO depletion in an aerobic condition in the presence of HbV, RBC, and EV

When the stock NO solution was simply injected into a PBS solution, the NO electrode showed an immediate increase to about 2000 nM, even in the aerobic condition. Then it gradually decreased according to the reaction of NO and O_2 to produce NO_2^- (Fig. 4). From the slope after 200 s, the apparent decay constant is calculated as 3.7×10^{-3} s^{-1}. In the case of the presence of EV, the increase in NO concentration immediately after injection and the decay curve were almost identical, and the apparent decay constant was 3.9×10^{-3} s^{-1}. From results of this experiment, it is not clear that the hydrophobic part of the lipid bilayer membrane facilitates NO depletion. The reactions of NO in the aqueous phase are still the prominent ones.

In the presence of HbV, the first injection of NO (2000 nM) was decayed much faster than the sensor was able to record, and only a part of the second NO injection was recorded. The decay curve was finally obtained at the third NO injection when the heme of HbV was totally inactivated with NO and converted to the ferric state. On the other hand, one injection of NO into the RBC suspension clearly showed the decay curve. However, the rate of decay is extremely fast, as indicated by the need for a different time scale of the abscissa. The NO decay constant of HbV was not obtained from this experiment, which has to be analyzed by stopped-flow spectrophotometry.

4. Discussion

Our primary finding is that NO binding is considerably retarded by encapsulation into phospholipid vesicles, and that CO binding is not influenced by encapsulation, but is slightly retarded by co-encapsulation with PLP as an allosteric effector. In the aerobic condition, the hydrophobic part of the lipid bilayer membrane does not seem to be involved in NO depletion (facilitated reaction with O_2), which is mostly attributable to the reaction with the intracellular Hb solution.

We recently showed that NO binding of Hb is retarded by encapsulation in phospholipid vesicles because of the intracellular diffusion barrier [23]. Intrinsically rapid NO binding causes Hb to become

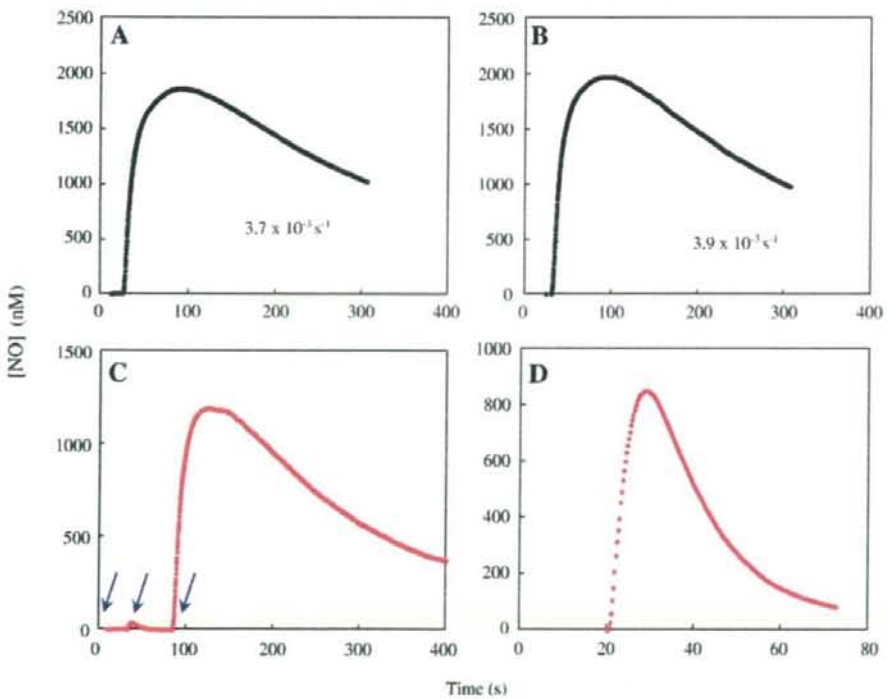

Fig. 4. NO decay in an aerobic condition in PBS solution after injection of NO yielding a concentration of 2000 nM NO. (A) PBS solution, as a standard curve of NO decay by the dissolved O_2. The decay rate is calculated as 3.7×10^{-3} s^{-1}. (B) PBS solution containing EV ([lipids] = 36 mg/mL). The decay rate is calculated as 3.9×10^{-3} s^{-1}. (C) PBS solution containing HbV ([heme] = 4 μM, [Hb] = 65 mg/L, [Lipid] = 36 mg/L). The arrows indicate the points of three injections. At the first and the second injections, HbV consumed NO so rapidly that the NO electrode was undetectable. At the third injection, Hb of HbV would be totally inactivated, and the NO level increased, and subsequently decreased gradually through reaction with the physically-dissolved O_2. (D) A PBS solution containing mice RBCs ([heme] = 3.72 μM). In contrast to HbV, the NO level increased at the first NO injection, although it did not reach to 2000 nM, and the NO decay was much faster than that in (A).

a sink of NO in the interior surface region of HbV, thereby hindering further NO diffusion into the core of HbV, in combination with the lowered diffusion constants of NO in a highly concentrated Hb solution. Using results described in a previous report, we compare two kinds of HbV with different P_{50} values (25 and 14 Torr), and showed that the $k'^{(NO)}_{on}$ might change slightly according to P_{50} (0.61×10^7 vs. 0.88×10^7 $M^{-1}s^{-1}$). Accordingly, the major cause of retardation is Hb encapsulation. Cell-free Hb removes NO much faster (cf. $k'^{(NO)}_{on}$ of cell-free Hb solution, $2.4–2.6\times10^7$ $M^{-1}s^{-1}$). Cell-free Hb solutions with and without PLP did not differ greatly. The results coincide well with those in precedent reports: that NO binding to α and β subunits and that the T-state and R-state Hbs are almost identical [36,37]. $Poly_BHb$ that contains high concentration of terameric $_BHb$ and intermolecularly crosslinked tetrameric $_BHb$ are known to induce vasoconstriction and hypertension [38]. In the present study, such $Poly_BHb$ showed identical rapid NO binding.

For CO, we previously reported that CO binding to Hb is intrinsically much slower than NO binding by two orders of magnitude, which allows more time for CO diffusion into the HbV core. Therefore, $k'^{(CO)}_{on}$ is not influenced by the intracellular Hb concentration and particle size smaller than 500 nm [23]. Results of the present study show the presence of a slight retardation of CO binding by HbV in comparison to the cell-free Hb solution, which is solely attributable to the co-encapsulation of PLP as an allosteric effector. The effector tends to stabilize the T-state and retards CO binding. In contrast to NO, it is well known that cooperative CO binding to four subunits of Hb occurs, and that the binding rate constants to α and β subunits, or T-state and R-state Hbs, are different [39,40]. According to Kwansa et al. [41], the value of $k^{(CO)}_{on}$ of unmodified $_BHb$ measured using stopped-flow is 1.3×10^5 $M^{-1}s^{-1}$. Polymerization of $_BHb$ by glutaraldehyde apparently facilitates CO binding ($k^{(CO)}_{on}$ of $Poly_BHb=2.7\times10^5$ $M^{-1}s^{-1}$).

In the circulation where O_2 is abundant NO is inactivated mainly by NO dioxygenation by O_2-bound HBOCs and RBC. Results of the present study confirmed that the cell-free human Hb solutions with our without PLP showed $k'^{(NO)}_{ox}$ of $7.4–8.7\times10^7$ $M^{-1}s^{-1}$, which was faster than that of the reaction of deoxyHb and NO ($k'^{(NO)}_{on}=2.4–2.6\times10^7$ $M^{-1}s^{-1}$), a tendency that coincided with the results of Herold et al. [42]. Encapsulation of HbO_2 in vesicles significantly retarded the reaction with NO, and $k'^{(NO)}_{ox}$ was 0.88×10^7 $M^{-1}s^{-1}$. However, we observed the change of heme ligation state ($HbO_2\rightarrow$metHb) and we were unable to observe the NO concentration using stopped-flow spectrophotometry. In an aerobic condition, NO reacts slowly with O_2 to produce NO_2^- in water.

The weight ratio of lipids to Hb of HbVs is about 0.5–0.6, this ratio being as low as 0.15 for RBCs. We anticipated that the hydrophobic part of the lipid bilayer membrane of HbV would be involved considerably in NO depletion, as reported by Liu et al. [24], which might affect the results of stopped-flow spectrophotometry. We monitored the NO decay in the presence of empty vesicles (without Hb) in an aerobic condition using a NO electrode to clarify the facilitation of NO depletion. Results show that NO decay in the presence of empty vesicles was almost identical to that in the PBS solution, indicating that the facilitated reaction of NO and O_2 in a hydrophobic part of the lipid bilayer membrane is negligibly small compared to the reaction with the intracellular Hb.

This finding may be related to the lipid composition of the membrane. The saturated phospholipid (DPPC, phase transition temperature = 41 °C) with cholesterol in HbV might be more resistant to oxidative damage than is soy phosphatidylcholine reported by Liu et al. [24], which probably contains many unsaturated fatty acids. Moreover, nitration of unsaturated bonds might occur, which is another pathway for NO depletion [43]. Conversely, our lipid mixture of DPPC comprises saturated fatty acids and cholesterol providing a hydrophobic rigid domain that would differ from the liposomes made of soy phospholipids. If the aqueous reaction of NO and dioxygen occurs with an overall stoichiometry of $4NO+O_2+2H_2O\rightarrow4H^++4NO_2^-$ [24,44], then H_2O is required even in the hydrophobic part. The unstable soy phospholipid vesicles in the literatures would provide more water molecules than does the rigid and stable bilayer membrane of our HbV. Accordingly, we conclude that NO depletion in aerobic conditions in the presence of HbV is caused primarily by the encapsulated Hbs, and the contribution of the bilayer membrane of HbV is negligibly small.

The NO decay in HbV was much faster than that for RBCs. In addition, measurements using the NO electrode were unable to detect the reaction rate of O_2-HbV and NO. These results demonstrate that NO mainly reacts with Hb in HbV. Given the rate of NO decay shown in Fig. 4, we can assume that less than 0.1% of total NO (1.9 μM) reacts with the physically-dissolved O_2 in PBS in 200 ms after the rapid mixing by stopped-flow spectrophotometry.

In a previous report on the relative magnitude of the binding rate constant of NO (fast) and CO (slow) to deoxygenated HbV, we predicted that the strength of the diffusion barrier induced in HbV becomes more significant with the faster ligand binding reaction with Hb [23]. According to our results and Herold et al. [42], the elementary reaction of NO and HbO_2 is much faster than that of NO with deoxyHb. As shown in Fig. 2, Hb encapsulation in vesicles retarded NO binding to deoxyHb by 1/4, and NO reaction with HbO_2 by 1/8. The impact of Hb encapsulation on the reaction with NO is strengthened in the aerobic condition.

We previously reported that HbV does not induce hypertension. However, present results, which show retardations of NO binding by encapsulation and CO binding by co-encapsulation of PLP in comparison to cell-free Hb solutions and $poly_BHb$, cannot fully explain the absence of vasoconstriction or hypertension after intravenous injection because these reactions of HbV are much greater than those of RBCs ($10^4–10^5$ M^{-1} s^{-1}) [1,2,37,45]. Any Hb-based oxygen carrier (HBOC) is much smaller than an RBC and is distributed homogeneously in the plasma layer [46]. Consequently, an RBC-free zone at the blood/endothelium interface becomes an HBOC-containing zone, and might be a sink of NO [47,48]. Rohlfs et al. [49] reported that NO binding rate constants of a series of chemically modified HBOCs (diameter, 6–28 nm), measured using the laser flash photolysis, were identical to that of an unmodified Hb solution: 3.0×10^7 $M^{-1}s^{-1}$. They concluded straightforwardly that NO uptake was unrelated to vasoconstriction because PEG-modified Hb did not induce vasoconstriction, other mechanisms being suggested as determinants of vasoconstriction such as molecular recognition, oxygen affinity [7,50] and facilitated diffusion. $Poly_BHb$ is larger than monomeric $_BHb$, but may be vasoactive because of the presence of monomeric $_BHb$ and its high P_{50} [25,31].

It is also speculated that there is a threshold particle diameter to penetrate across the perforated endothelial cell layer to approach a space (such as the space of Disse near the sinusoidal endothelial layer

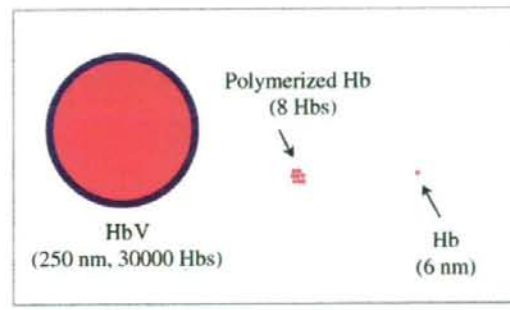

Fig. 5. Comparison of particle size between HbV (250 nm), Hb (6 nm) and polymerized Hb. According to the molecular weight distribution of $Poly_BHb$ [31], the molecular weight (Mw) of the largest polymerized Hb is 502 kDa, which corresponds to 8 Hbs. One HbV contains about 30,000 Hbs. It is obvious that HbV is much larger than the largest fraction of $Poly_BHb$. For the retardation of NO binding, both Hb concentration in the particle and the particle size are important [23].

in a hepatic microcirculation, or the space between the endothelium and the smooth muscle), where CO or NO is produced as a vasorelaxation factor. Because the particle size of HbV (250 nm) is obviously much larger than the Hb tetramer and its polymerized form as shown in Fig. 5 both the retardation of NO reaction and the larger particle diameter are inferred to be keys to suppress vasoconstriction and hypertension induced by HBOCs.

In conclusion, the source of vasoactivity of HBOCs has been extensively reviewed [7,9,13,38,51–54] and it is generally agreed that NO scavenging is a factor in this process, although it does not provide an all encompassing explanation. In terms of HbV, the intrinsically fast reactions of NO with the cell-free Hb solutions in both aerobic and anaerobic conditions are considerably retarded by the encapsulation process. Therefore, since NO bioavailability results from the balance of the rate of NO production and NO entrapment or scavenging, the finding that the latter processes are significantly retarded in HbVs provides some meaningful information to explain their vasoinactivity.

Acknowledgements

The authors would like to thank Dr. Hirohisa Horinouchi (Keio University), Dr. Amy G. Tsai and Dr. Pedro Cabrales (University of California, San Diego), and Dr. Keitaro Sou (Waseda University) for valuable discussions. This work was supported in part by the grant for the Health Sciences Research including Drug Innovation from the Ministry of Health, Labour and Welfare, Japan, Grants in Aid for Scientific Research (B) from the Japan Society for the Promotion of Science (19300164), and USPHS Bioengineering Research Partnership grant R24-HL 64395, R01-HL62354 and P01-HL71064.

References

[1] E. Carlsen, J.H. Comroe, The rate of uptake of carbon monoxide and of nitric oxide by normal human erythrocytes and experimentally produced spherocytes, J. Gen. Physiol. 42 (1958) 83–107.
[2] X. Liu, M.J. Miller, M.S. Joshi, H. Sadowska-Krowicka, D.A. Clark, J.R. Lancaster Jr., Diffusion-limited reaction of free nitric oxide with erythrocytes, J. Biol. Chem. 273 (1998) 18709–19713.
[3] M.W. Vaughn, K.T. Huang, L. Kuo, J.C. Liao, Erythrocytes possess an intrinsic barrier to nitric oxide consumption, J. Biol. Chem. 275 (2000) 2342–2348.
[4] P.C. Minneci, K.J. Deans, H. Zhi, P.S. Yuen, R.A. Star, S.M. Banks, A.N. Schechter, C. Natanson, M.T. Gladwin, S.B. Solomon, Hemolysis-associated endothelial dysfunction mediated by accelerated NO inactivation by decompartmentalized oxyhemoglobin, J. Clin. Invest. 115 (2005) 3409–3417.
[5] J.R. Hess, V.W. MacDonald, W.W. Brinkley, Systemic and pulmonary hypertension after resuscitation with cell-free hemoglobin, J. Appl. Physiol. 74 (1993) 1769–1778.
[6] E.P. Sloan, M. Koenigsberg, D. Gens, M. Cipolle, J. Runge, M.N. Mallory, G. Rodman Jr., Diaspirin cross-linked hemoglobin (DCLHb) in the treatment of severe traumatic hemorrhagic shock: a randomized controlled efficacy trial, JAMA 282 (1999) 1857–1864.
[7] A. Gulati, A. Barve, A.P. Sen, Pharmacology of hemoglobin therapeutics, J. Lab. Clin. Med. 133 (1999) 112–119.
[8] G. Rochon, A. Caron, M. Toussaint-Hacquard, A.I. Alayash, M. Gentils, P. Labrude, J.F. Stoltz, P. Menu, Hemodilution with stroma-free hemoglobin at physiologically maintained viscosity delays the onset of vasoconstriction, Hypertension 43 (2004) 1110–1115.
[9] H. Sakai, H. Hara, M. Yuasa, A.G. Tsai, S. Takeoka, E. Tsuchida, M. Intaglietta, Molecular dimensions of Hb-based O_2 carriers determine constriction of resistance arteries and hypertension, Am. J. Physiol. Heart Circ. Physiol. 279 (2000) H908–H915.
[10] K. Nakai, T. Ohta, I. Sakuma, K. Akama, Y. Kobayashi, S. Tokuyama, A. Kitabatake, Y. Nakazato, T.A. Takahashi, S. Sekiguchi, Inhibition of endothelium-dependent relaxation by hemoglobin in rabbit aortic strips: comparison between acellular hemoglobin derivatives and cellular hemoglobins, J. Cardiovasc. Pharmacol. 28 (1996) 115–123.
[11] J.S. Olson, E.W. Foley, C. Rogge, A.L. Tsai, M.P. Doyle, D.D. Lemon, NO scavenging and the hypertensive effect of hemoglobin-based blood substitutes, Free Radic. Biol. Med. 36 (2004) 685–697.
[12] M. Suematsu, N. Goda, T. Sano, S. Kashiwagi, T. Egawa, Y. Shinoda, Y. Ishimura, Carbon monoxide: an endogenous modulator of sinusoidal tone in the perfused rat liver, J. Clin. Invest. 96 (1995) 2431–2437.
[13] N. Goda, K. Suzuki, M. Naito, S. Takeoka, E. Tsuchida, Y. Ishimura, T. Tamatani, M. Suematsu, Distribution of heme oxygenase isoforms in rat liver. Topographic basis for carbon monoxide-mediated microvascular relaxation, J. Clin. Invest. 101 (1998) 604–612.
[14] X. Liu, A. Samouilov, J.R. Lancaster Jr., J.L. Zweier, Nitric oxide uptake by erythrocytes is primarily limited by extracellular diffusion not membrane resistance, J. Biol. Chem. 277 (2002) 26194–26199.
[15] D.B. Kim-Shapiro, A.N. Schechter, M.T. Gladwin, Unraveling the reactions of nitric oxide, nitrite, and hemoglobin in physiology and therapeutics, Arterioscler. Thromb. Vasc. Biol. 26 (2006) 697–705.
[16] K.T. Huang, Z. Huang, D.B. Kim-Shapiro, Nitric oxide red blood cell membrane permeability at high and low oxygen tension, Nitric Oxide 16 (2007) 209–216.
[17] K.T. Huang, T.H. Han, D.R. Hyduke, M.W. Vaughn, H. Van Herle, T.W. Hein, C. Zhang, L. Kuo, J.C. Liao, Modulation of nitric oxide bioavailability by erythrocytes, Proc. Natl. Acad. Sci. U. S. A. 98 (2001) 11771–11776.
[18] T.H. Han, A. Pelling, T.J. Jeon, J.K. Gimzewski, J.C. Liao, Erythrocyte nitric oxide transport reduced by a submembrane cytoskeletal barrier, Biochim. Biophys. Acta 1723 (2005) 135–142.
[19] J.T. Coin, J.S. Olson, The rate of oxygen uptake by human red blood cells, J. Biol. Chem. 254 (1979) 1178–1190.
[20] L. Djordjevich, I.F. Miller, Synthetic erythrocytes from lipid encapsulated hemoglobin, Exp. Hematol. 8 (1980) 584–592.
[21] E. Tsuchida, H. Sakai, H. Horinouchi, K. Kobayashi, Hemoglobin-vesicles as a transfusion alternative, Artif. Cells Blood Substit. Biotechnol. 34 (2006) 581–588.
[22] H. Sakai, K. Hamada, S. Takeoka, H. Nishide, E. Tsuchida, Functional evaluation of hemoglobin- and lipidheme-vesicles as red cell substitutes, Polymer Adv. Technol. 7 (1996) 639–644.
[23] H. Sakai, A. Sato, K. Masuda, S. Takeoka, E. Tsuchida, Encapsulation of concentrated hemoglobin solution in phospholipid vesicles retards the reaction with NO, but not CO, by intracellular diffusion barrier, J. Biol. Chem. 283 (2008) 1508–1517.
[24] X. Liu, M.J. Miller, M.S. Joshi, D.D. Thomas, J.R. Lancaster Jr., Accelerated reaction of nitric oxide with O_2 within the hydrophobic interior of biological membranes, Proc. Natl. Acad. Sci. U. S. A. 95 (1998) 2175–2179.
[25] P.W. Buehler, R.A. Boykins, Y. Jia, S. Norris, D.I. Freedberg, A.I. Alayash, Structural and functional characterization of glutaraldehyde-polymerized bovine hemoglobin and its isolated fractions, Anal. Chem. 77 (2005) 3466–3478.
[26] H. Sakai, S. Takeoka, H. Yokohama, Y. Seino, H. Nishide, E. Tsuchida, Purification of concentrated hemoglobin using organic solvent and heat treatment, Protein Expr. Purif. 4 (1993) 563–569.
[27] H. Sakai, Y. Masada, S. Takeoka, E. Tsuchida, Characteristics of bovine hemoglobin as a potential source of hemoglobin-vesicles for an artificial oxygen carrier, J. Biochem. (Tokyo) 131 (2002) 611–617.
[28] S. Takeoka, T. Ohgushi, K. Terase, T. Ohmori, E. Tsuchida, Layer-controlled hemoglobin vesicles by interaction of hemoglobin with a phospholipid assembly, Langmuir 12 (1996) 1755–1759.
[29] K. Sou, Y. Naito, T. Endo, S. Takeoka, E. Tsuchida, Effective encapsulation of proteins into size-controlled phospholipid vesicles using freeze–thawing and extrusion, Biotechnol. Prog. 19 (2003) 1547–1552.
[30] L. Wang, K. Morizawa, S. Tokuyama, T. Satoh, E. Tsuchida, Modulation of oxygen-carrying capacity of artificial red cells, Polymers Adv. Technol. 4 (1993) 8–11.
[31] P. Cabrales, A.G. Tsai, M. Intaglietta, Increased tissue PO_2 and decreased O_2 delivery and consumption after 80% exchange transfusion with polymerized hemoglobin, Am. J. Physiol. Heart Circ. Physiol. 287 (2004) H2825–H2833.
[32] J. Herzfeld, N.E. Seidel, M.P. Taylor, P.R. Droupadi, N.E. Wang, Gentle chemical deoxygenation of hemoglobin solutions, Hemoglobin 14 (1990) 399–411.
[33] C.A. Sawicki, Q.H. Gibson, Tetramer–dimer dissociation of carboxyhemoglobin in the absence of dithionite, Biophys. J. 35 (1981) 265–270.
[34] I. Gramaglia, P. Sobolewski, D. Meays, R. Contreras, J.P. Nolan, J.A. Frangos, M. Intaglietta, H.C. van der Heyde, Low nitric oxide bioavailability contributes to the genesis of experimental cerebral malaria, Nat. Med. 12 (2006) 1417–1422.
[35] H. Sakai, K. Tomiyama, Y. Masada, S. Takeoka, H. Horinouchi, K. Kobayashi, E. Tsuchida, Pretreatment of serum containing hemoglobin vesicles (oxygen carriers) to prevent their interference in laboratory tests, Clin. Chem. Lab. Med. 41 (2003) 222–231.
[36] R. Cassoly, Q. Gibson, Conformation, co-operativity and ligand binding in human hemoglobin, J. Mol. Biol. 91 (1975) 301–313.
[37] J.S. Olson, Stopped-flow, rapid mixing measurements of ligand binding to hemoglobin and red cells, Methods Enzymol. 76 (1981) 631–651.
[38] P. Pawson, I.F. Gibson, F.J. Dowell, The effect of the polymerized bovine haemoglobin solution, Hb-200, on endothelial function in isolated arterial rings from rats, J. Vet. Pharmacol. Therap. 30 (2007) 556–563.
[39] M. Brunori, J. Bonaventura, C. Bonaventura, E. Antonini, J. Wyman, Carbon monoxide binding by hemoglobin and myoglobin under photodissociating conditions, Proc. Natl. Acad. Sci. U. S. A. 69 (1972) 868–871.
[40] M. Perrella, N. Davids, L. Rossi-Bernardi, The association reaction between hemoglobin and carbon monoxide as studied by the isolation of the intermediates. Implications on the mechanism of cooperativity, J. Biol. Chem. 267 (1992) 8744–8751.
[41] H.E. Kwansa, A.D. Young, D. Arosio, A. Razynska, E. Bucci, Adipyl crosslinked bovine hemoglobins as new models of allosteric systems, Proteins 39 (2000) 166–169.
[42] S. Herold, M. Exner, T. Nauser, Kinetic and mechanistic studies of the NO*-mediated oxidation of oxymyoglobin and oxyhemoglobin, Biochemistry 40 (2001) 3385–3395.
[43] P.R. Baker, Y. Lin, F.J. Schopfer, S.R. Woodcock, A.L. Groeger, C. Batthyany, S. Sweeney, M.H. Long, K.E. Iles, L.M. Baker, B.P. Branchaud, Y.E. Chen, B.A. Freeman, Fatty acid transduction of nitric oxide signaling: multiple nitrated unsaturated fatty acid derivatives exist in human blood and urine and serve as endogenous peroxisome proliferator-activated receptor ligands, J. Biol. Chem. 280 (2005) 42464–42475.
[44] P.C. Ford, D.A. Wink, D.M. Stanbury, Autoxidation kinetics of aqueous nitric oxide, FEBS Lett. 326 (1993) 1–3.
[45] I. Azarov, K.T. Huang, S. Basu, M.T. Gladwin, N. Hogg, D.B. Kim-Shapiro, Nitric oxide scavenging by red blood cells as a function of hematocrit and oxygenation, J. Biol. Chem. 280 (2005) 39024–39032.
[46] H. Sakai, Y. Suzuki, M. Kinoshita, S. Takeoka, N. Maeda, E. Tsuchida, O_2 release from Hb vesicles evaluated using an artificial, narrow O_2-permaeble tube: comparison with RBCs and acellular Hbs, Am. J. Physiol. Heart Circ. Physiol. 285 (2003) H2543–H2555.

[47] M. Kavdia, N.M. Tsoukias, A.S. Popel, Model of nitric oxide diffusion in an arteriole: impact of hemoglobin-based blood substitutes, Am. J. Physiol. Heart Circ. Physiol. 282 (2002) H2245–H2253.
[48] A. Jeffers, M.T. Gladwin, D.B. Kim-Shapiro, Computation of plasma hemoglobin nitric oxide scavenging in hemolytic anemias, Free Radic. Biol. Med. 41 (2006) 1557–1565.
[49] R.J. Rohlfs, E. Bruner, A. Chiu, A. Gonzales, M.L. Gonzales, D. Magde, M.D. Magde Jr., K.D. Vandegriff, R.M. Winslow, Arterial blood pressure responses to cell-free hemoglobin solutions and the reaction with nitric oxide, J. Biol. Chem. 273 (1998) 12128–12134.
[50] A.G. Tsai, P. Cabrales, B.N. Manjula, S.A. Acharya, R.M. Winslow, M. Intaglietta, Dissociation of local nitric oxide concentration and vasoconstriction in the presence of cell-free hemoglobin oxygen carriers, Blood 108 (2006) 3603–3610.
[51] K. Nakai, I. Sakuma, T. Ohta, J. Ando, A. Kitabatake, Y. Nakazato, T.A. Takahashi, Permeability characteristics of hemoglobin derivatives across cultured endothelial cell monolayers, J. Lab. Clin. Med. 132 (1998) 313–319.
[52] Y. Smani, A. Fifre, P. Labrude, C. Vigneron, B. Faivre, Pharmacological and physicochemical factors in the pressor effects of conjugated haemoglobin-based oxygen carriers in vivo, J. Hypertens. 25 (2007) 599–608.
[53] D.H. Doherty, M.P. Doyle, S.R. Curry, R.J. Vali, T.J. Fattor, J.S. Olson, D.D. Lemon, Rate of reaction with nitric oxide determines the hypertensive effect of cell-free hemoglobin, Nat. Biotechnol. 16 (1998) 672–676.
[54] B. Matheson, H.E. Kwansa, E. Bucci, A. Rebel, R.C. Koehler, Vascular response to infusions of a nonextravasating hemoglobin polymer, J. Appl. Physiol. 93 (2002) 1479–1486.

Am J Physiol Gastrointest Liver Physiol 295: G664–G670, 2008.
First published July 24, 2008; doi:10.1152/ajpgi.90316.2008.

The role of luminal factors in the recovery of gastric function and behavioral changes after chronic *Helicobacter pylori* infection

Elena F. Verdu,[1]* Premysl Bercik,[1]* Xian Xi Huang,[1] Jun Lu,[1] Nafia Al-Mutawaly,[1] Hiromi Sakai,[2] Thomas A. Tompkins,[3] Kenneth Croitoru,[1] Eihun Tsuchida,[2] Mary Perdue,[1] and Stephen M. Collins[1]

[1]*Intestinal Disease Research Program, McMaster University, Hamilton, Ontario, Canada;* [2]*Advanced Research Institute for Science and Engineering, Waseda University, Tokyo, Japan; and* [3]*Institut Rosell-Lallemand, Montreal, Quebec, Canada*

Submitted 2 May 2008; accepted in final form 20 July 2008

Verdu EF, Bercik P, Huang XX, Lu J, Al-Mutawaly N, Sakai H, Tompkins TA, Croitoru K, Tsuchida E, Perdue M, Collins SM. The role of luminal factors in the recovery of gastric function and behavioral changes after chronic *Helicobacter pylori* infection. *Am J Physiol Gastrointest Liver Physiol* 295: G664–G670, 2008. First published July 24, 2008; doi:10.1152/ajpgi.90316.2008.—The role of chronic infections, such as *Helicobacter pylori* (*Hp*), to produce sustained changes in host physiology remains controversial. In this study, we investigate whether the antigenic or bacterial content of the gut, after *Hp* eradication, influences the changes in gut function induced by chronic *Hp* infection. Mice were infected with *Hp* for 4 mo and then treated with antibiotics or placebo for 2 wk. Gastric emptying was measured using videofluoroscopy, feeding behavior using a 24-h feeding system, and intestinal permeability using an isolated jejunal segment arterially perfused with an artificial oxygen carrier, hemoglobin vesicles. Immune responses were assessed by $CD3^+$ cell counts and anti-*Hp* antibodies using ELISA. To determine the role of luminal factors in host physiology posteradication, groups of mice received the probiotics containing *Lactobacillus rhamnosus* R0011 and *L. helveticus* R0052 or placebo for 2 wk or crude *Hp* antigen weekly for 2 mo. Chronic *Hp* infection was associated with delayed gastric emptying, increased intestinal permeability, and increased gastric $CD3^+$ cell counts. *Hp*-induced altered feeding patterns did not reverse after eradication. Probiotics accelerated the recovery of paracellular permeability and delayed gastric emptying, improved the $CD3^+$ cell counts, and normalized altered feeding patterns posteradication. *Hp* antigen resulted in increased anti-*Hp* antibodies and increased $CD3^+$ cell counts in the stomach and delayed recovery of gastric function. Our results suggest that the bacterial content of the gut, as well as the presence of relevant antigens, influences the rate of recovery of host pathophysiology induced by chronic *Hp* infection. These changes do not seem to occur in association with modulation of intestinal permeability.

lactobacilli; gastric emptying; feeding patterns

CONTROVERSY SURROUNDS THE ROLE of chronic *Helicobacter pylori* (*H. pylori*) infection as a cause of functional dyspepsia. Although it is known that *H. pylori* infection can alter gastric physiology, clinical evidence shows that there is little, if any, relief of symptoms following successful eradication of the bacterium in the short or medium term (4, 11, 16, 20, 21). The notion that acute bacterial infection can trigger a sequence of events resulting in chronic gastrointestinal symptomatology has now been established in the context of acute gastroenteritis as a trigger of both irritable bowel syndrome and functional dyspepsia (12, 17–19, 23). Less is known about the role of chronic infections, such as *H. pylori*, and their ability to produce sustained changes in host physiology and possibly persistent symptoms.

Chronic gastric inflammation is the hallmark of *H. pylori* infection (7, 13). We have shown that, in mice, *H. pylori* infection induces functional and morphological changes in the gastric and spinal neural circuitry that are progressive and lymphocyte dependent (2). Some of these changes persist after bacterial eradication, suggesting that postinfective changes and immune activation are long lasting. In particular, altered feeding patterns, reminiscent of early satiety, are present up to 2 mo posteradication (posteradication) (3).

Persistence of symptoms may relate to luminal factors, which maintain low-grade inflammation after *H. pylori* eradication. Gut barrier function is crucial in limiting the effect of luminal antigens on the immune system. Thus, in this study, we examined whether the antigenic or bacterial content of the gut influences the changes in gastric function and feeding behavior induced by the *H. pylori* chronic infection. Specifically, we determined whether exposure to *H. pylori* antigen or probiotic bacteria influences host physiology.

Our results suggest that the bacterial content of the gut, as well as the presence of relevant antigens, influences the rate of recovery of host pathophysiology induced by *H. pylori* infection.

MATERIALS AND METHODS

Animals. Male BALB/c mice (Harlan, Indianapolis, IN) were purchased at the age of 6–8 wk and housed in a conventional specific pathogen-free unit at McMaster University Central Animal Facility. All experiments were conducted with approval from the McMaster University Animal Care Committee.

Chronic H. pylori infection. Mice chronically infected with *H. pylori* Sydney strain for 4 mo ($n = 64$) and a group of uninfected controls were used ($n = 27$). Additional mice infected with *H. pylori* were used to monitor the establishment of a chronic infection ($n = 14$). Every 2 wk, beginning at 2 wk postinfection, 2 mice per group were euthanized, and *H. pylori* infection was verified using Warthin-Starry staining. Gastric emptying and 24-h feeding patterns were assessed at 4 mo of chronic infection. Additional mice were euthanized and used for ex vivo intestinal permeability measurements. *H. pylori* eradication therapy was administered thereafter using antibiotic-containing food pellets (Bio-Serv, Frenchtown, NJ) for 2 wk. Gastric emptying was reassessed 2 wk and 2 mo posteradication. Feeding patterns and intestinal permeability were reassessed 2 mo posteradication.

Inflammation. Stomach samples (Swiss rolls) were preserved in 10% formalin and then stained with hematoxylin and eosin (H & E).

* E. Verdu and P. Bercik contributed equally to this work.

Address for reprint requests and other correspondence: E. F. Verdu, McMaster Univ. HSC 3N49C, 1200 Main St. West, Hamilton, Ontario, Canada (e-mail: verdue@mcmaster.ca).

The costs of publication of this article were defrayed in part by the payment of page charges. The article must therefore be hereby marked "*advertisement*" in accordance with 18 U.S.C. Section 1734 solely to indicate this fact.

H & E-stained and Warthin-Starry-stained slides were examined under light microscopy to confirm *H. pylori* eradication after antimicrobial therapy and assess gastric inflammation. Mononuclear cell (MN) scores were graded in the corpus on a scale of 0–3 as described previously (2).

Immunostaining for $CD3^+$ cells was performed on stomach paraffin sections using a modified method described previously (2). Rabbit anti-mouse CD3 (1:300; Dako, Glostrup, Denmark) was used as primary antibody followed by biotinylated swine anti-rabbit (1:300, Dako) and streptavidin peroxidase conjugate (1:600, Dako). The antibodies were visualized using 3-amino-9-ethylcarbazole and counterstaining with Mayers hematoxylin. Negative controls were performed in the absence of primary antibody. $CD3^+$ cells were counted in two slides per mouse (n = 12/group) and averaged. $CD3^+$ cells present in three randomly selected fields in the corpus and antrum separately (x63, mucosa and submucosa) were counted. Samples from the jejunal loop were obtained at the end of each permeability experiment to test for tissue viability. Samples were fixed in 10% formalin, stained with H & E, and examined for tissue damage as a result of hypoxia using light microscopy. Gross villous architecture and the presence of cell desquamation and edema at villi tips were investigated.

H. pylori antibody measurement. Levels of anti-*H. pylori* IgG1 and IgG2A were measured at 2 mo posteradication by ELISA using biotinylated goat anti-mouse IgG2a and IgG1 (Southern Biotechnology Associates, Birmingham, AL) as described previously (9).

Gastric emptying. Mice were gavaged with 0.2 ml of 40% barium and placed in a custom-made restrainer. Videofluoroscopic images of stomach were taken at 0 and 4 min and stored for offline analysis using VCR (Panasonic). Video images were then digitized and analyzed using public domain NIH Image 1.62 software (developed at the U.S. National Institutes of Health). Gastric emptying was calculated by multiplying the area of stomach by mean optical density of the gastric area and was expressed as a percentage of barium expelled in 4 min.

Twenty-four-hour feeding patterns. Twenty-four-hour feeding patterns were assessed individually in mice placed in the separate cages. Food pellets were fastened on the feeding tray positioned 5 cm above the bottom of the cage, which was connected to the strain gauge placed above the cage. The weight of the feeding tray with food pellets was continuously recorded by computer. Data acquisition and analysis were performed using custom designed software (written by N. Al-Mutawaly). The number of feeding episodes, amount of food per episode, and total amount of food consumed was calculated. An eating bout was defined as an episode of food consumption lasting more than 20 s; two bouts were considered to be independent from each other if the interval of quiescence was longer than 5 min.

Intestinal permeability. Intestinal permeability ex vivo was investigated using an isolated arterially perfused jejunal loop (1, 22). Briefly, a 4-cm segment of the distal jejunum was selected, and a terminal branch of the superior mesenteric artery was cannulated with a polyethylene catheter under intraperitoneal ketamine/xylazine anesthesia. Tissue oxygenation was maintained by perfusion of the arterial branch with hemoglobin vesicles (Waseda University, Tokyo, Japan) (17a) using a peristaltic pump (Ismatec, Zurich, Switzerland). Luminal ends of the jejunal segment were cannulated using polyethylene cannulas. Following gentle washing of the lumen with saline to remove food residue, the jejunal loop was dissected and transferred to a custom-built organ chamber containing saline at 37°C. The loop was then perfused intraluminally with saline at 5 ml/h by using a syringe infusion pump (Harvard University, Boston, MA). All preparations were allowed to equilibrate for 5 min before collection of venous outflow, which was sampled continuously for the entire duration of the experiment (36 min) in 3-min fractions. Intestinal segment was perfused luminally with isosmotic mixture of ^{51}Cr-EDTA (0.6 μCi/ml) and ^{14}C-mannitol (0.1 μCi/ml) (Perkin Elmer, Boston, MA) solution for 9 min at 5 ml/h. After the end of each experiment, two full-thickness tissue samples were excised from proximal and distal regions of the loop and fixed in formalin for later microscopic examination. Concentration of the radiolabeled macromolecules in the venous outflow was detected using a liquid scintillation Beta counter (LS 5801; Beckman Coulter, Mississauga, ON, Canada). The recovery of radioactivity in each venous outflow fraction is expressed as a proportion of that found in an identical volume of the luminal perfusate.

H. pylori antigen administration posteradication. To maintain persistence of gastric dysfunction posteradication a group of mice received crude *H. pylori* antigen (100 μg/mouse) by gavage once weekly for 2 mo starting 1 wk after *H. pylori* eradication therapy. *H. pylori* antigen was prepared from fresh *H. pylori* cultures using liquid brain-heart infusion-based media as described previously (2). The bacteria were then gently centrifuged, and pellets were resuspended in saline and homogenized/disrupted with a sonicator. The concentration of bacterial antigen was adjusted with saline (100 μl/mouse). Gastric emptying was reassessed at the end of *H. pylori* antigen administration (2 mo posteradication). Stomach samples were obtained at sacrifice and fixed in formalin for Warthin-Starry stain and for $CD3^+$ cell counts.

Probiotic treatment posteradication. Groups of mice received by daily gavage either 100 μl of placebo-maltodextrin dissolved in sterile water or 100 μl of 10^{10} *Lactobacillus rhamnosus* (*L. rhamnosus*) R0011 and *L. helveticus* R0052 (Lacidofil) for 2 wk immediately after eradication therapy. Uninfected mice received maltodextrin treatment on a daily basis for 2 wk. Gastric emptying was reassessed at the end of probiotic treatment (2 wk posteradication) and at 2 mo posteradication. Fecal pellets were obtained at 2 wk to investigate probiotic survival in the gastrointestinal tract. Twenty-four-hour feeding patterns were reexamined at 2 mo posteradication. Additional mice were euthanized for ex vivo permeability measurements at 2 mo posteradication.

Detection of L. rhamnosus R0011 and L. helveticus R0052 in feces. Fresh fecal pellets were collected aseptically from the anal region into a sterile cryogenic tube containing 0.9% saline and 10% glycerol while the animals were kept in Plexiglas restrainers. For analysis, 100 μl of fecal solution were pipetted into 25 ml of de Man, Rogosa, and Sharpe broth plus antibiotics (5.9 mg/ml phosphomycin and 18.6 mg/ml sulfamethoxazole) and 1 mg/ml in H_2SO_4 0.02 M trimethoprim. Vancomycin (5 mg) was added for selective *L. rhamnosus* R0011 and ciprofloxacin (5 mg) for *L. helveticus* R0052 growth and was cultured anaerobically at 37°C for 48 h.

For DNA extraction and PCR amplification, 1.5 ml of each culture solution were centrifuged, and bacteria pellet was collected. Bacterial genomic DNA was extracted by Wizard Genomic DNA purification kit (Promega, Madison, WI) according to manufacturer's instructions. PCR amplification was performed in a DNA Thermal Cycler 480 (Perkin Elmer) as follows: in a 0.5 ml PCR tube, 1 μl (0.2 μg) of DNA was added to 49 μl of PCR reaction mixture containing 200 μM of each dNTP, 1.5 mM $MgCl_2$, 10 pmol amounts of each primer and 2.5 U of Taq DNA. PCR cycling parameters were 3 min at 94°C followed by 30 cycles of 30 s at 94°C, 30 s at 55°C, 60 s at 72°C; after the last cycle, we added a final extension 7 min at 72°C. PCR product was visualized by ethidium bromide staining in 2% agarose gels. R0011 was used as a positive control, and L. *casei* R0215 were used as negative controls.

PCR primer pairs were as follows: *L. helveticus* R0052: sense 5′-ATTTTGCAACT GTTACTCCATC-3′, antisense 5′-GCATAATAGTCTTAGCTACGC-3′; *L. rhamnosus* R0011 (two pairs of primer sets): sense 5′-GACAATACTGATTTCCACC-3′, antisense 5′-TCCAATGTTCTCAACCAG-3′ and sense TCAGTAGACACCTACCGG-3′, antisense 5′-GTTGTAAAAGCTCTGGGACGCG. The first pair of primers can amplify *L. zeae* ATCC 393 and its prophage (phiAT3) due to the high homology between this phage and R0011

prophage, LarhR11-1. Therefore, only samples that were positive for both primer sets were considered positive for R0011.

Statistical analysis. Data are presented as means ± SD or medians with interquartile ranges when appropriate. Data was analyzed using either two-way ANOVA, Kolmogorov-Smirnov test or non-paired *t*-test as appropriate. The Spearman rank correlation test was used to test the strength of association between parameters. A P value of <0.05 was considered statistically significant.

RESULTS

Effect of chronic H. pylori infection on inflammation. Chronic *H. pylori* infection (4 mo postinfection) induced chronic active inflammation, located mainly in the submucosal layer of the proximal stomach. The mononuclear cell score in the corpus was 0.6 ± 0.6 and 2.0 ± 0.7 ($P < 0.01$) in uninfected controls and *H. pylori*-infected mice, respectively. $CD3^+$ cell scores in controls were 3.8 ± 3.0 and 0.8 ± 0.9 in corpus and antrum, respectively. During *H. pylori* infection, they increased to 14.3 ± 7.1 and 4.5 ± 1.2 (both $P < 0.01$ vs. uninfected controls).

Effect of chronic H. pylori infection on gastric emptying. In accordance with previous results (3), the percentage of retained barium during *H. pylori* infection was 30% higher than in uninfected mice (Fig. 1, before eradication). Gastric emptying fully normalized at 2 mo posteradication (Fig. 1, 2 mo after eradication).

Effect of chronic H. pylori infection on body weight. In accordance with previous results (2, 3), there were no differences in body weight between uninfected and chronically *H. pylori*-infected mice (24.3 ± 2.6 g and 24.7 ± 3.0 g, respectively).

H. pylori antigen delays recovery of inflammation and gut function after bacterial eradication. In mice previously infected with *H. pylori*, administration of crude *H. pylori* antigen maintained delayed gastric emptying for up to 2 mo posteradication (Fig. 1, 2 mo posteradication). Delayed gastric emptying correlated with increased $CD3^+$ cell counts (Spearman rank correlation test, $P < 0.05$). Antigen-treated mice had IgG1 and IgG2A values nine- and 23-fold higher, respectively, compared with placebo-treated mice. Antigen administration did not affect gastric emptying in uninfected mice.

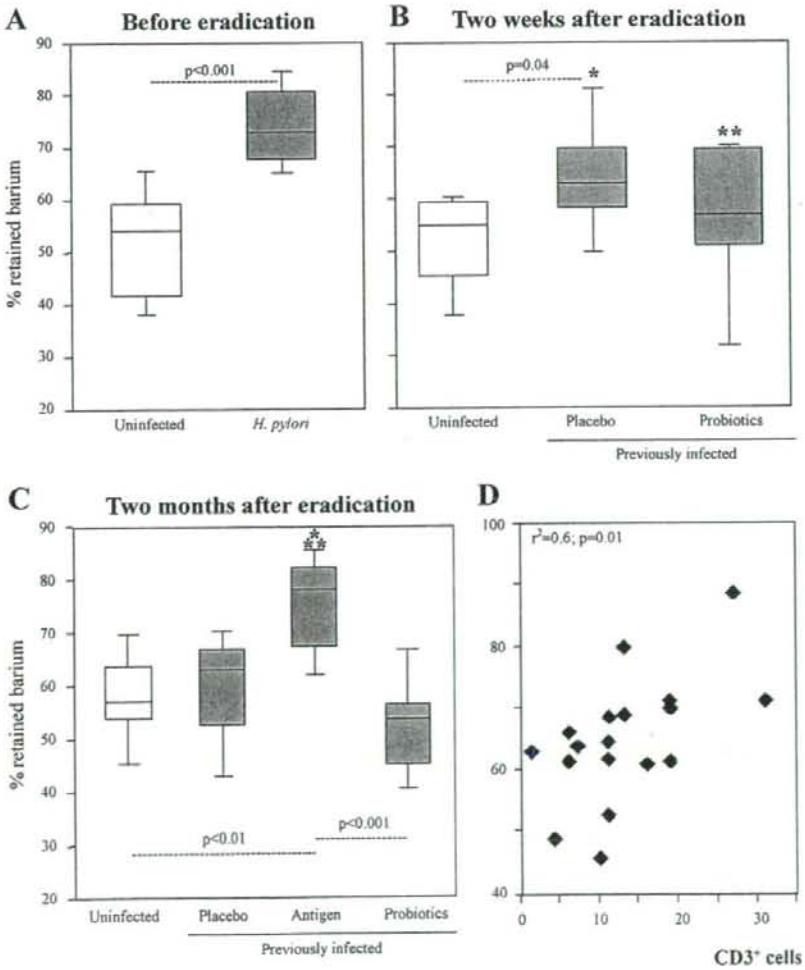

Fig. 1. *A*: gastric emptying was delayed in mice infected with *Helicobacter pylori* (*H. pylori*) ($n = 36$) compared with uninfected controls ($n = 20$). *B*: two weeks after eradication, gastric emptying improved in previously infected mice treated with placebo ($n = 12$, $*P = 0.02$ vs. *H. pylori*) but remained delayed compared with uninfected controls ($P = 0.04$). Previously infected mice treated with probiotics ($n = 12$) improved their gastric emptying ($**P < 0.01$ vs. *H. pylori*) and were similar to uninfected controls but were not different from placebo-treated mice. *C*: two months posteradication, gastric emptying normalized in placebo-treated ($n = 12$) mice but remained abnormal in antigen-treated mice ($n = 12$, $*P < 0.01$ vs. uninfected antigen, $**P = 0.02$ vs. uninfected placebo). *D*: degree of delayed gastric emptying was associated with the $CD3^+$ cell counts in stomach (r^2, 0.6; $P = 0.01$).

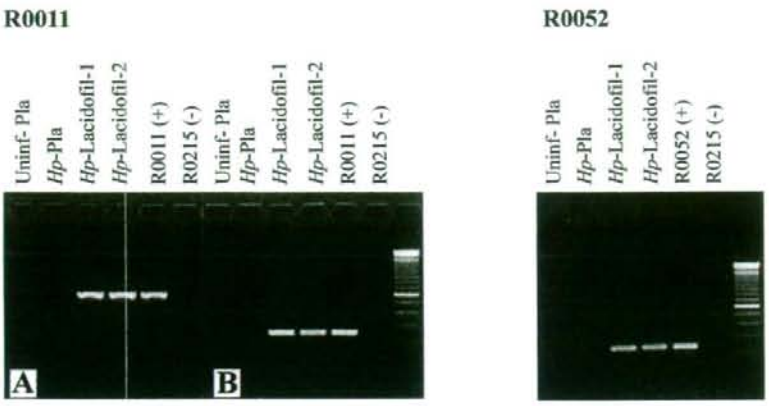

Fig. 2. Example of PCR detection of probiotics in feces. Two primers were used to detect R0011 (*A* and *B*) and one primer to detect R0052. Bands show negative detection of probiotics in feces of uninfected mice treated with maltodextrin (Uninf-pla), infected mice treated with maltodextrin placebo (Hp-Pla), and negative control R0215. Positive detection is shown in 2 infected mice treated with probiotics (Hp-Lacidofil-1 and -2), and in positive controls using R0011 and R0052.

Detection of L. rhamnosus R0011 and L. helveticus R0052 in feces. Figure 2 shows an example of positive detection for *L. rhamnosus* R0011 and *L. helveticus* R0052 in feces at the end of probiotic feeding. All Lacidofil-fed mice tested positive for the specific probiotics in feces at the end of the probiotic administration period. No cross contamination was observed in mice gavaged with placebo.

Probiotics improve markers of inflammation posteradication. In placebo-treated mice, there was persistent infiltration with $CD3^+$ T cells in the submucosal layer of the corpus and antrum 2 mo after eradication of *H. pylori*. In contrast, previously infected mice treated with probiotics exhibited a 60% lower MN score in corpus compared with placebo-treated mice (2.2 ± 0.5 vs. 0.8 ± 0.4, $P = 0.01$). The $CD3^+$ T cell infiltrate in both corpus and antrum was also reduced by probiotic therapy (Fig. 3). There was no overt inflammation in the jejunal segments of *H. pylori*-infected mice compared with uninfected controls.

Effect of probiotics on gastric emptying after H. pylori eradication. At 2 wk posteradication, previously *H. pylori*-infected mice treated with probiotics had returned to uninfected

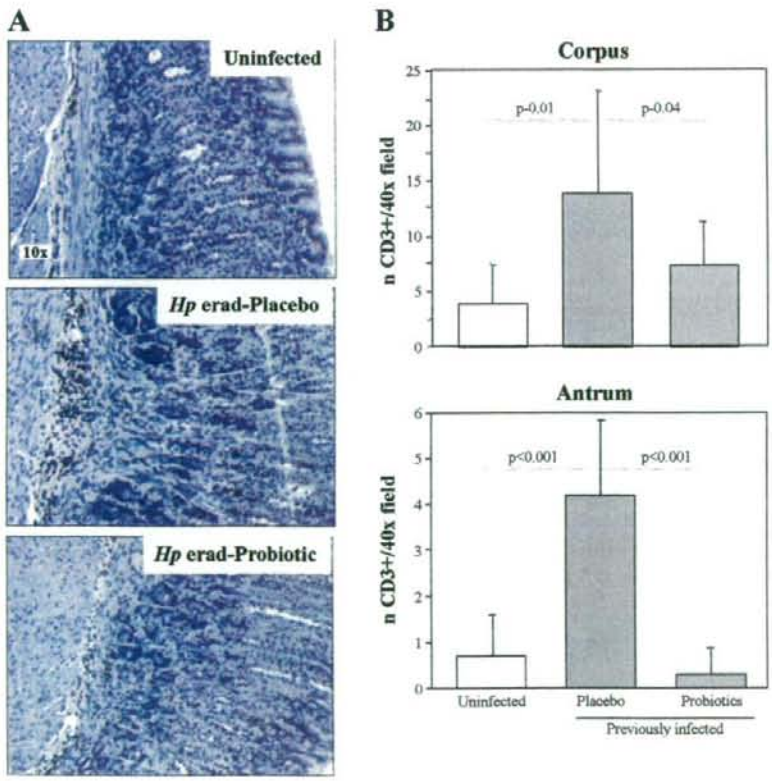

Fig. 3. *A*: at 2 mo posteradication, a persistent, predominantly submucosal chronic infiltrate was observed in the gastric body of mice previously infected with *H. pylori* compared with uninfected controls. Treatment with probiotics decreased chronic gastritis (photograph magnification ×10). *B*: $CD3^+$ cell counts were increased both in corpus ($P = 0.01$) and antrum ($P < 0.0001$) of previously infected mice compared with uninfected controls. Treatment with probiotics normalized the $CD3^+$ cell counts in both corpus and antrum ($P = 0.04$ and $P < 0.001$ vs. placebo-treated mice). Quantification performed in mucosa and submucosa; 2 slides/mouse ($n = 12$/group) (magnification ×63) and averaged.

gastric emptying values. However, there were no statistical differences between previously infected mice treated with placebo or probiotics 2 wk after eradication. Two months after eradication, previously infected mice that had been treated with probiotics tended to have faster gastric emptying than placebo-treated mice (Fig. 1).

Probiotics improve recovery of 24-h feeding behavior after H. pylori eradication. At 4 mo, frequency of eating bouts per 24 h was higher in *H. pylori*-infected mice compared with uninfected controls (Fig. 4). In placebo-treated mice, altered feeding patterns remained unchanged for at least 2 mo posteradication. In contrast, previously infected mice treated with probiotics had a similar number of eating bouts per 24 h as uninfected time-point controls.

Effect of probiotics on paracellular small intestinal permeability. Only intestinal segments with intact morphology at the end of experiments were included in the study. Jejunal permeability to ^{51}Cr-EDTA and ^{14}C-mannitol was increased in *H. pylori*-infected mice compared with uninfected controls (Fig. 5). Bacterial eradication combined with probiotics tended to improve paracellular permeability to ^{51}Cr-EDTA ($P = 0.35$ vs. uninfected controls), but this did not reach statistical significance vs. placebo-treated mice. Probiotics did not affect membrane permeability as assessed by ^{14}C-mannitol.

DISCUSSION

The aim of our study was to investigate whether the antigenic or bacterial content of the gut influences the rate of recovery of host physiology induced by chronic *H. pylori* infection after bacterial eradication.

We have previously shown that altered gastric emptying improves at 2 wk posteradication and completely normalizes 2 mo posteradication (3). The probiotic combination *L. rhamnosus* R0011 and *L. helveticus* R0052 administered immediately after *H. pylori* eradication accelerated recovery of gastric chronic inflammation. In contrast, previously infected mice that received *H. pylori* antigen had persistent CD3$^+$ cell counts in the stomach that correlated with persistent delayed gastric emptying posteradication.

In the chronic model of *H. pylori* infection, the degree of neural impairment is proportional to the extent of the chronic inflammatory infiltrate (2). In the present study, we have extended this observation and showed that the degree of delayed gastric emptying is proportional to the CD3$^+$ cell counts in the stomach. Furthermore, *H. pylori* antigen-treated mice had persistent delayed gastric emptying posteradication compared with placebo-treated controls. This was accompanied by higher anti-*H. pylori* antibody titers, suggesting a

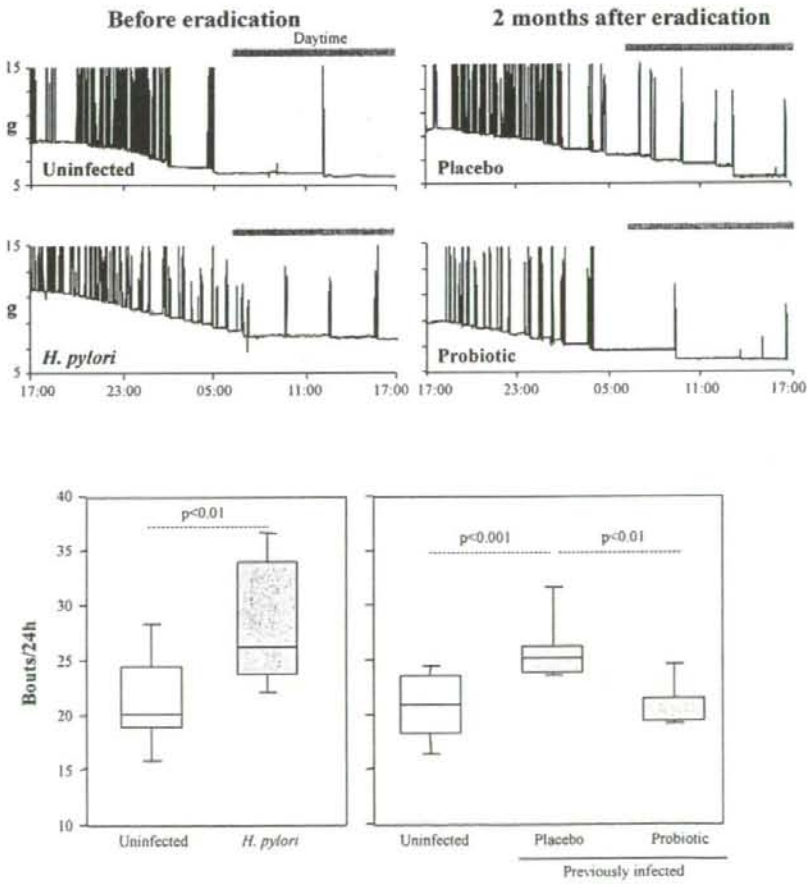

Fig. 4. Examples of feeding patterns in control ($n = 8$) and *H. pylori*-infected mice ($n = 16$). Control mice fed almost exclusively during nighttime. *H. pylori*-infected mice fed frequently during the day time as well. The abnormal feeding pattern persisted until 2 mo posteradication in placebo-treated mice ($n = 8$), whereas it normalized in probiotic-treated mice ($n = 8$). The number of feeding bouts was increased in *H. pylori*-infected mice compared with controls. Two months posteradication, the number of feeding bouts normalized in probiotic-treated mice but not in placebo-treated mice.